# P-T path determinations in the Tormes Gneissic Dome, NW Iberian Massif, Spain

J. ESCUDER VIRUETE, I A. INDARES AND R. ARENASr

**ABSTRACT** The Tormes Gneissic Dome (TGD, NW sector of the Iberian Massif, Spain) is a high-grade metamorphic complex affected by a major episode of extensional deformation (D2). The syn-D2 *P–T* path of the Lower Unit of the TGD was deduced from the analysis of reaction textures related to superimposed fabrics developed during exhumation, analysis of mineral zoning and thermobarometric calculations. It comprises an initial phase of decompression, determined using the TWEEQU thermobarometric technique, from 6.4–8.1 kbar at 735–750 °C (upper structural levels) and 7.2 kbar at 770 °C (lower structural levels) to 3.3–3.9 kbar and 645–680 °C. This evolution is consistent with the observed sequence of melting reactions and the generation of garnet- and cordierite-bearing anatectic granitoids. The later part of the syn-D2 *P–T* path consisted of almost isobaric cooling associated with the thermal re-equilibration of the unit in the new structural position. This segment of the *P–T* path is recorded by assemblages with And + Bt + Ms and Ms + Chl + Ab related to the later mylonitic S2 fabrics, which indicate retrogression to low-amphibolite and greenschist facies conditions.

**Key words:** crustal extension; garnet zoning; high-temperature decompression; Iberian Massif; melting; metapelite; *P–T* path.

## INTRODUCTION

Recent developments in thermobarometric techniques (Essene, 1989), in the numerical modelling of chemical zoning in metamorphic minerals (Spear & Selverstone, 1983; Spear, 1989, 1993) and in the theoretical aspects of *P–T–t* metamorphic paths (Thompson & England, 1984; Nisbet & Fowler, 1988; Peacock, 1989) have resulted in great progress in understanding the relationships between tectonics and metamorphism in orogenic areas. However, in high-grade terranes, mineral assemblages are prone to pervasive resetting during the initial stages of cooling, due to enhanced diffusion under high-*T* conditions. Therefore, rigorous criteria have to be used to evaluate whether peak compositions are preserved, otherwise calculated *P–T* conditions may be erroneous (Lasaga, 1983; Frost & Chacko, 1989; Selverstone & Chamberlain, 1990; Spear, 1991; Spear & Florence, 1992). In addition, independent constraints may be placed by careful textural interpretations and use of appropriate petrogenetic grids. Taking all this into account, the determination of *P–T* paths in high-grade complexes is a powerful tool that can provide essential information on the thermal and tectonic evolution of deep crustal levels during orogenic processes.

This paper deals with the interpretation of textures and mineral zoning, and application of thermobarometry to a suite of high-grade metapelites and felsic orthogneisses collected in the Lower Unit of the Tormes Gneissic Dome (TGD), NW Salamanca (Spain). These data are used to deduce an important part of the tectonothermal evolution of the gneissic ensemble. The *P–T* conditions and *P–T* paths were first constrained by using textural relationships and appropriate petrogenetic grids. In order to select points for thermobarometry, different factors that can affect the validity of the calculations were taken into account, such as garnet size, cooling rates, the nature of the reactions operative in the sample during exhumation and the amounts and compositional trends of other phases that may react with garnet at any time (Spear & Florence, 1992). *P–T* conditions were calculated with the TWEEQU software (Berman, 1991), which uses an internally consistent thermodynamic database. In the last section the tectonometamorphic implications of the *P–T* paths obtained and their relationship with the recently recognized Hercynian extensional deformation in the TGD are discussed.

## GEOLOGICAL SETTING

### Regional framework

The Tormes Gneissic Dome (TGD) is located in the NW sector of the Iberian Massif (Fig. 1), which represents the westernmost segment of the European Hercynian Belt. This sector has been divided into four zones (Julivert *et al.*, 1972; Arenas *et al.*, 1986, 1995) with different geological characteristics: the Cantabrian

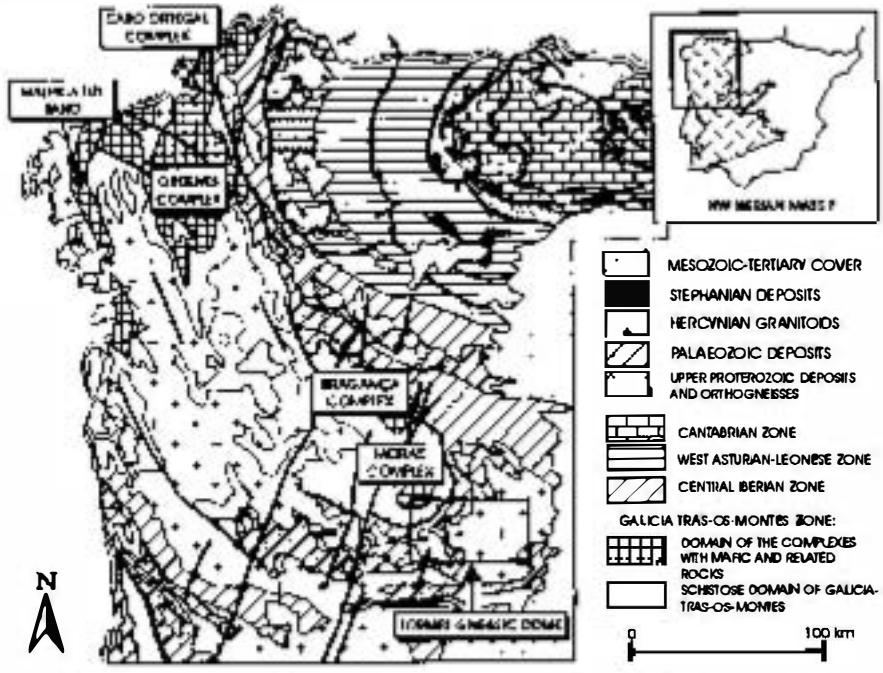


**Fig. 1.** Location of the studied area in a schematic geological map of the Hercynian belt in the NW of the Iberian Peninsula (after Arenas *et al.*, 1986).

(CZ), the West Asturian–Leonese (WALZ) and the Central Iberian Zones (CIZ), which are parautochthonous, and the Galicia Trás-os-Montes Zone (GTMZ), which is allochthonous over the CIZ. The Hercynian collision led to the stacking of these tectonic units, which migrated over time from the innermost zones of the CIZ to the foreland of the CZ (Pérez Estaún *et al.*, 1991; Arenas *et al.*, 1995). The CIZ is characterized by extensive granitic plutonism and by the presence of high-grade metamorphic complexes, one of which is the TGD. In this complex, earlier Hercynian contractional fabrics are overprinted by a major extensional event (Escuder Viruete *et al.*, 1994). This tectonic setting is not exclusive to the TGD, but has also been described in other parts of the CIZ (Diez Balda *et al.*, 1992, 1995; Doblas *et al.*, 1994; Escuder Viruete *et al.*, 1994).

### The metamorphic complex

The Tormes Gneissic Dome (TGD) is a complex late Hercynian structure (Figs 2 & 3) with a broad domal shape, as indicated by the general outward dips of the main metamorphic foliation, elongated in the NW–SE and W–E directions. It consists of two lithotectonic units, separated by an extensional tectonic contact (Escuder Viruete *et al.*, 1994). The Upper Unit comprises a monotonous sequence of slates and quartzites, whose upper levels have been dated as Lower Cambrian, which is unconformably overlain by an Ordovician–Silurian sequence of anchimetamorphic and epizonal fossiliferous sediments. To the northwest, the Upper Unit underlies the allochthonous GMTZ. The Lower Unit comprises a high-grade metamorphic complex mainly composed of augen gneisses (618 ± 9 Ma, U/Pb on zircon; Lancelot *et al.*, 1985) and migmatized felsic orthogneisses and metapelites with lenses of marble and calcsilicate rocks. The TGD was intruded by two types of granitic rocks: (1) biotite and two-mica peraluminous granitoids with abundant metasedimentary enclaves, which are mainly concentrated in the inner parts of the structural dome; and (2) biotite meta-aluminous granodiorites and subordinate tonalites with hornblende-bearing dioritic xenoliths that occur in the Upper Unit. Isotopic data suggest intrusion ages of *c.* 325–318 Ma for both types of granitoids (Serrano Pinto & Gil Ibarguchi, 1987).

In the TGD, the extensional deformation resulted in a set of regionally consistent D2 structures which overprint earlier D1 contractional structures. The major D2 extensional feature in the dome is a several kilometres thick, low-angle crustal-scale shear zone, characterized by ductile S/L fabrics. The two units are separated by narrower and steeper ductile detachments, with normal movement, which developed under lower-grade metamorphic conditions and are considered to have formed during the later stages of the same event. Both the major shear zone and the lower-grade detachments display evidence of top to the SE tectonic transport, which gave rise to the final juxtaposition of the Upper Unit over the Lower Unit (Escuder Viruete *et al.*, 1994). The final geometry of the TGD results from the superposition of later structures, including a set of open antiforms and synforms related to a moderate D3 contractional event, a system of ENE–WSW-trending strike-slip sinistral shear zones, and a

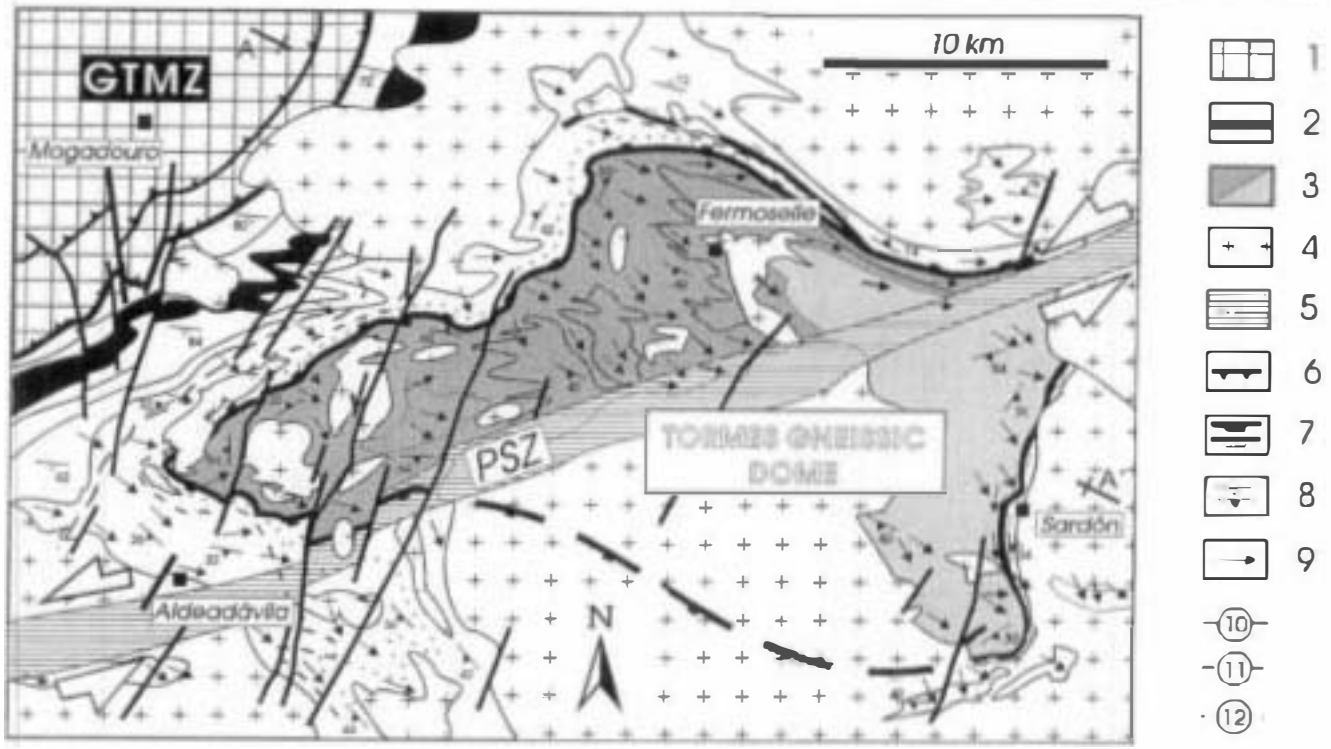


**Fig. 2.** Geological map of the Tormes Gneissic Dome. (1) Galicia-Trás-os-Montes Zone (GTMZ); includes allochthonous complexes with ophiolites and units with high-*P* metamorphism. (2) Upper Unit (Upper Precambrian to Lower Devonian sequences; in black, the Lower Ordovician Armorican Quartzite). (3) Lower Unit; light grey, sector below the extensional shear zone. (4) Synkinematic Hercynian granitoids (syn- and post-M2). (5) Late transcurrent shear zone (PSZ = Pereña Shear Zone), for which the large white arrows indicate the sense of shear. (6) Hercynian thrust fault. (7) Low-grade detachment zones. (8) Direction and dip of the S1 schistosity (open triangles) and the S2 mylonitic foliation (solid triangles). (9) Direction of the L2 stretching lineation and movement of the hangingwall. M2 isograds: (10) andalusite (+); (11) sillimanite (+); (12) sillimanite + K-feldspar (+).

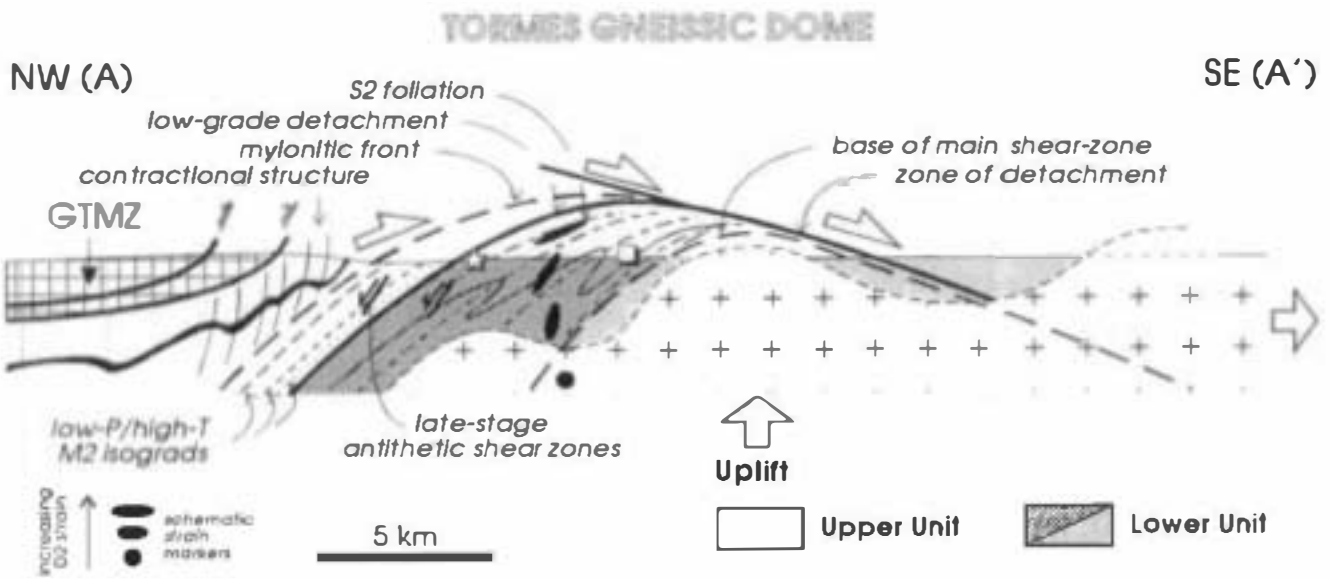


**Fig. 3.** Schematic cross-section of the Tormes Gneissic Dome parallel to the direction of extension, showing the structural relationships between units with different tectonometamorphic evolution. With the progressive doming process the main shear zone rotated towards the NW and was cut at a low angle by a late detachment zone of normal movement towards the SE. The star indicates the location of paragneiss samples belonging to the upper structural levels of the Lower Unit, whereas the square indicates those belonging to the lower levels. For the sake of clarity, the late transcurrent Pereña Shear Zone is not shown.

system of ductile–brittle and brittle D4 NW–SE- to E–W-trending normal faults (Escuder Viruete, 1995).

In both units, the thermal peak of metamorphism was attained during the D2 extensional event (M2) and variably obliterated earlier contractional Barrovian metamorphic signatures (M1, Escuder Viruete, 1995). The Upper Unit displays a condensed sequence of M2 isograds (originally defined by Martínez, 1974), parallel to the contact with the Lower Unit, up to low-*P* amphibolite facies conditions (Fig. 2, Escuder-Viruete *et al.*, 1994). The Lower Unit attained metamorphic conditions of high-*T* amphibolite transitional to mid-*P* granulite facies, with the development of partial melting (Gil Ibarguchi & Martínez, 1982; Martínez *et al.*, 1988; López Plaza y Gonzalo, 1993; Escuder Viruete *et al.*, 1994). The age of M2 and D2 is constrained by the 325–318 Ma ages of emplacement of the granitoids, which are syn- to post-S2 (Escuder Viruete, 1995).

## METAMORPHISM OF METAPELITES AND FELSIC ORTHOGNEISSES IN THE LOWER UNIT

### Textures and mineralogy

Metapelites and felsic orthogneisses of the Lower Unit are characterized by the mineral assemblage Grt–Bt–Kfs–Sil–Pl–Qt±Ilm (mineral abbreviations after Kretz, 1983), considered to represent the thermal peak. They also display syn-S2 textures, whose timing of development relative to the M2 metamorphic evolution depends upon their structural position relative to the main shear zone. Three main types of syn-S2 textures were recognized: those formed during the thermal peak, those associated with the early stages of retrogression and those related to deformation under low-grade metamorphic conditions (Fig. 4).

The central part of the structural dome is characterized by coarse-grained granoblastic S2 fabrics that define the main foliation. The metapelites display alternating biotite–sillimanite-rich domains and quartz-rich lenses with aggregates of garnet, plagioclase, K-feldspar, prismatic sillimanite and minor ilmenite, apatite and zircon. In both types of rocks garnet is idio–subidioblastic, up to 1 cm in diameter, shows stable contacts against the K-feldspar and, in some cases, contains inclusions of biotite, plagioclase, quartz, ilmenite and, rarely, rutile (Fig. 5e). Since the latter is absent from the matrix, it is interpreted as a relict prograde phase and therefore it is not included in the mineral assemblage of the thermal peak. Quartz occurs as recrystallized (annealed) ribbons that are parallel to the mesoscopic L2. This texture indicates that the D2 deformation occurred close to the thermal peak, and is in agreement with evidence of development of prograde syn-D2 reaction textures, such as garnet and K-feldspar porphyroblasts growing over an early S2 foliation defined by Bt + Sil + Qtz (Fig. 5a), in which the sillimanite crystals define L2.

The middle structural levels of the Lower Unit are characterized by protomylonitic and mylonitic S2 fabrics of type II S–C (Lister & Snoke, 1984) and post-date the thermal peak. In the metapelites, garnet porphyroblasts are partially replaced, in pressure shadows and syn-D2 pull-aparts, by cordierite coronas together with quartz (Fig. 5b), and fine intergrowths of Sil + Bt ± Pl ± Ilm (Fig. 5c), or are variably pseudomorphed by Bt + Qtz ± Pl ± Ilm aggregates (Fig. 5f & g). These porphyroblasts are preserved in sigmoidal quartz-rich microdomains surrounded by Bt + Sil + Ilm-rich bands that define the C–S fabric. Fibrolitic sillimanite is stable in both the S and C surfaces, but fibrolite nematoblasts, parallel to L2, are boudinaged, with pull-aparts filled with biotite. All these textures are consistent with the retrograde nature of the S2 fabric at these levels. Quartz occurs as an interpenetrative mosaic of equant grains that define ribbons parallel to L2 and show conjugate grain-boundary alignments resulting from high-*T* migration of grain boundaries during deformation (600–700°C; Lister & Snoke, 1984). This microtexture, together with the extensive recrystallization of plagioclase, suggests that D2 deformation took place under medium/high-*T* amphibolite facies conditions, and can be considered to record the onset of cooling during D2.

In the upper structural levels of the Lower Unit, the D2 retrograde effects are progressively more intense. Development of lower-grade assemblages in S2 fabrics includes partial replacement of sillimanite by andalusite and of K-feldspar by muscovite. In the detachment zone between the two units, the S2 foliation is locally overprinted by an extensional crenulation cleavage (ECC; Platt & Vissers, 1980). These crenulation cleavage zones are located at low angles (20–30°) to the S2 surfaces of the main mylonitic foliation and display evidence of normal movement. In the planar structures of the ECC the Qtz + Ms + Chl + Fe–Ti oxides ± Bt assemblage is stable, indicating greenschist facies conditions. In these fabrics (Fig. 5d), recrystallization of quartz took place by progressive rotation of subgrains, feldspar porphyroclasts are partially replaced by Ms + Qtz aggregates and biotite porphyroclasts reveal internal deformation and variable chloritization.

### Interpretation

The mineral assemblages presented above, together with evidence of partial melting and the characteristics of the leucosomes, can be used to constrain metamorphic *P–T* conditions at the thermal peak and the subsequent *P–T* path. Moreover, two generations of peraluminous leucogranites, one with garnet and one with cordierite, have been identified in the Lower Unit on the basis of their petrographic and structural characteristics (Escuder Viruete, 1995). Their genesis can be interpreted in relation to the melting curves crossed during different stages of the *P–T* path.

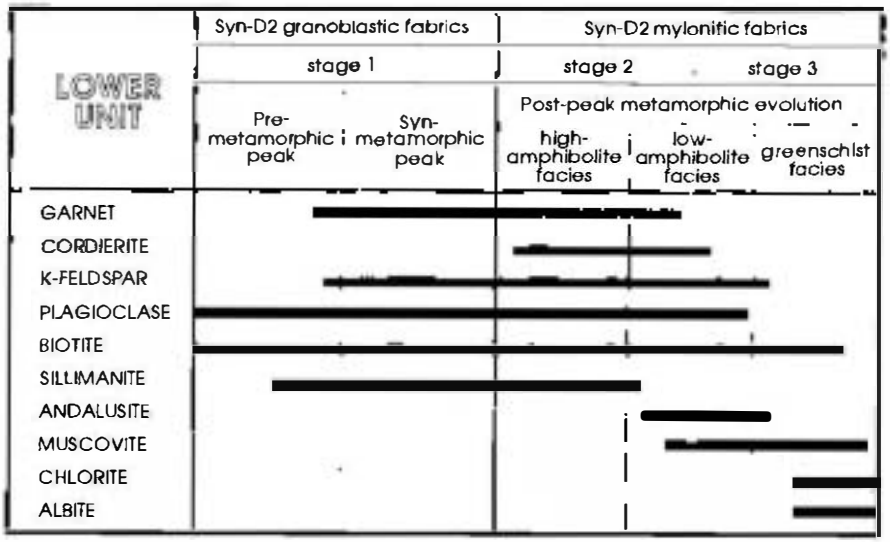


**Fig. 4.** Summary of the observed relationships between growth of mineral phases and evolution of S2 fabrics in metapelitic gneisses of the Lower Unit of the Tormes Gneissic Dome. Black lines indicate growth of new minerals and grey lines indicate their recrystallization.

Relevant reactions in the KMFASH system (after Vielzeuf & Holloway, 1988) and the proposed $P$–$T$ path are shown in Fig. 6.

The coexistence of Sil + Kfs in the peak assemblage indicates temperature conditions above the dehydration melting of muscovite according to the reaction (Fig. 6)

$$\text{muscovite} + \text{quartz}(+\text{plagioclase}) \rightarrow \text{sillimanite} + \text{K-feldspar} + \text{melt}. \quad \text{(R1)}$$

In addition, the presence of leucocratic segregations with garnet in some metapelites suggests that, locally, the reaction

$$\text{biotite} + \text{sillimanite} + \text{quartz}(+\text{plagioclase}) \rightarrow \text{garnet} + \text{K-feldspar} + \text{melt} \quad \text{(R2)}$$

also occurred. Reaction (R2) produces a large amount of melt in rocks of pelitic composition (Vielzeuf & Holloway, 1988), and may be responsible for the garnetiferous leucogranites in the TDG, which exhibits a magmatic foliation concordant with the S2 of the country rock. The location of these two reactions in $P$–$T$ space depends upon the presence or absence of plagioclase and on its composition, and to a minor extent on the $X_{Mg}$ of the rock (Vielzeuf & Holloway, 1988). For common plagioclase-bearing metapelitic rocks, reactions (R1) and (R2) occur at 680–740 °C (between 6 and 10 kbar) and 750 °C, respectively (Le Breton & Thompson, 1988), but they are shifted to higher temperatures by a few tens of degrees in plagioclase-free systems (Vielzeuf & Holloway, 1988). On the other hand, an upper $T$ limit may be placed by the absence of orthopyroxene from the study area, implying that the temperature was not high enough for the next dehydration melting reaction,

$$\text{biotite} + \text{quartz}(+\text{plagioclase}) \rightarrow \text{orthopyroxene} + \text{K-feldspar} + \text{melt}, \quad \text{(R3)}$$

to occur. For typical metapelites, this reaction is crossed at 800 °C (Spear 1993, figs 10–16).

The presence of sillimanite places an upper $P$ limit between 8 and 10 kbar in the range 700–800°C. On the other hand, the absence of cordierite from the peak assemblage suggests that pressure conditions were above the upper $P$ limit of the divariant reaction

$$\text{sillimanite} + \text{garnet} + \text{quartz} + H_2O \rightarrow \text{cordierite}. \quad \text{(R4)}$$

Reaction (R4) has a relatively flat slope in $P$–$T$ space in the KFMASH system ($dP/dT = 0.203$ kbar/100 °C, calculated with the $P$–$TX$ software, Perkins *et al.*, 1987) and metamorphic cordierite is not normally stable in metapelites at pressures above 6 kbar (Lonker, 1981; Aranovich & Podlesskii, 1983). However, this mineral replaces garnet in the middle and upper structural levels as a syn-D2 retrograde product of reaction (R4), indicating decompression during the initial stages of retrogression. Moreover, cordierite also appears in metapelites of the lower structural levels, forming part of some leucocratic segregations that are concordant with the S2 foliation. This cordierite is generated by the reaction

$$\text{biotite} + \text{sillimanite} + \text{quartz} \pm \text{plagioclase} \rightarrow \text{cordierite} + \text{K-feldspar} + \text{melt}, \quad \text{(R5)}$$

and it is present as a magmatic phase in a second generation of structurally late and post-D2 peralumi-

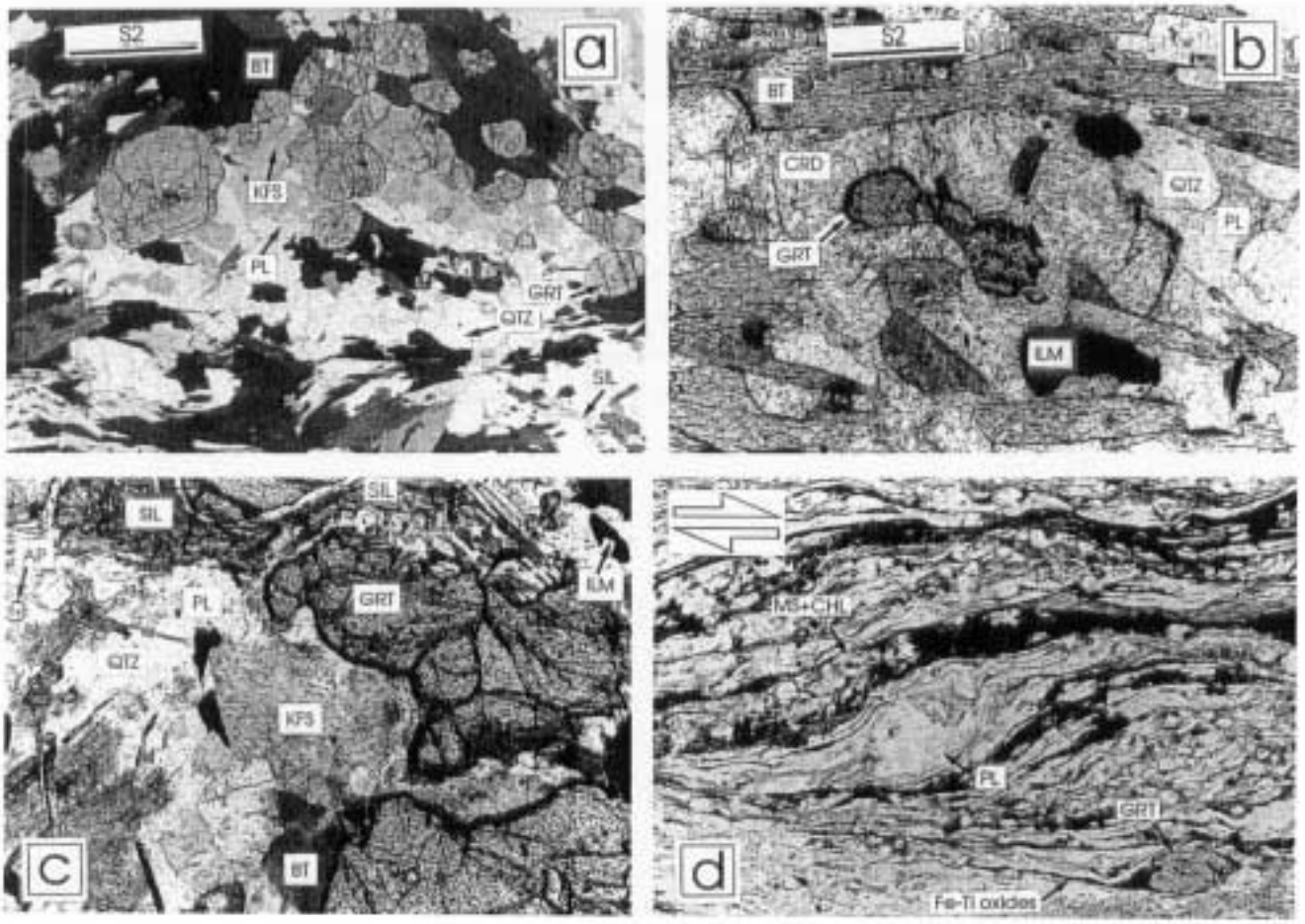


Fig. 5. Microfabrics developed during D2 in the metapelites of the Lower Unit of the TGD. All the photomicrographs are with plane polarized light. (a) Syn-S2 granoblastic microfabric formed during the thermal peak. The stable mineral assemblage is Grt + Kfs + Pl + Qtz + Bt + Sil. Note the development of Grt + Kfs over an early S2 foliation defined by Bt + Qtz + Sil. Width of photo = 5 mm. (b) Crd + Ilm growth after Grt + Bt. Width of photo = 1 mm. (c) Replacement of garnet by intergrowths of Bt–Sil–Pl–Qtz–Ilm–Ap during retrogression. The star shows Bt + Pl + Qtz + Sil symplectites in a garnet rim. Width of photo = 1 mm. (d) Syn-S2 S–C mylonitic microfabric of type II developed in low-grade detachment zones. S2 is defined by bands consisting of 'ribbon' quartz alternating with darker bands rich in micas and Fe–Ti oxide. The asymmetry of the S–C fabric and of the porphyroclasts of plagioclase (centre) and garnet (lower right) is dextral. Note that S2 Bt is variably transformed to a Ms + Chl aggregate. Width of photo = 5 mm. (e) Mineral assemblage developed in felsic orthogneisses during the thermal peak of M2. Garnet-bearing quartzofeldspathic aggregate (Qtz + Kfs + Pl) parallel to the S2 foliation defined by Bt + Sil. Garnet (Grt) includes rutile (Rt) in the core and ilmenite (Ilm) towards the rim area. A–B: location of the chemical profile shown in Fig. 8. Width of photo = 10 mm. (f) Mineral assemblage developed in metapelites after the thermal peak of M2. The S2 foliation is defined by garnet-bearing quartzofeldspathic aggregates surrounded by biotite and sillimanite prisms parallel to L2. Note the retrograde replacement of garnet by Qtz + Bt + Pl aggregates. A–B: location of the chemical profile shown in Fig. 6(b). Width of photo = 6.3 mm. (g) Detail of the previous photo showing the retrograde replacement of garnet by an aggregate of Qtz + Bt + Pl in contact with the matrix minerals. Width of photo = 3.5 mm.

nous leucogranites. Reaction (R5) also has a relatively flat slope in $P$–$T$ space (Clemens & Wall, 1981; Vielzeuf & Holloway, 1988), and occurs at ≈4 kbar between 700 and 750 °C. The above information indicates that the rocks followed a steep retrograde $P$–$T$ path which entered the stability field of cordierite and led to the development of peraluminous granitic melts (Clemens & Wall, 1981; Vielzeuf & Holloway, 1988) by anatexis at low pressures during advanced stages of the syn-D2 decompression.

Additional evidence of syn-D2 decompression is given by the replacement of garnet by Bt + Pl + Qtz aggregates (Fig. 5f & g), indicating the retrograde reaction

$$\text{garnet} + \text{K-feldspar} + \text{H}_2\text{O} \rightarrow \text{biotite} + \text{quartz} + \text{plagioclase}, \qquad \text{(R6)}$$

which has a positive slope in $P$–$T$ space ($dP/dT$ = 0.714 kbar/100 °C in the model KFMASH system calculated with the $P$–$TX$ software of Perkins *et al.*, 1987).

On the other hand, the existence of subsolidus mylonitic S2 fabrics that affect the garnet-bearing

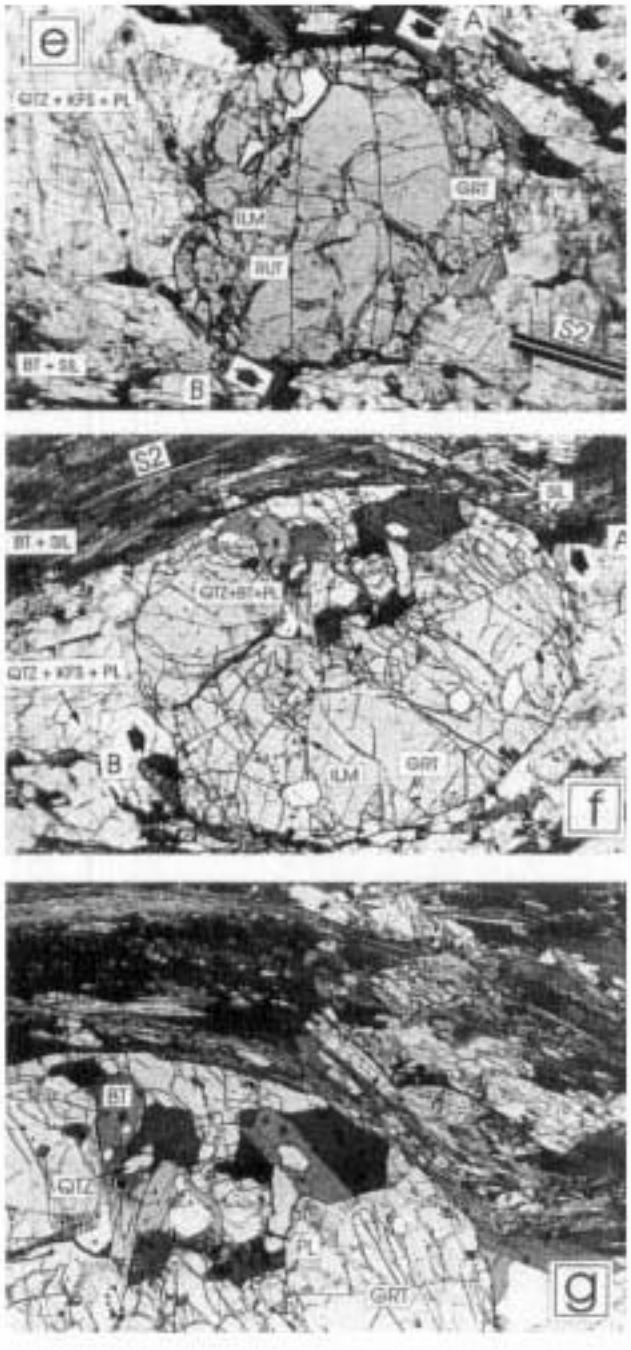


leucogranites and are subparallel to the earlier magmatic fabrics is evidence for the progressive cooling that took place during D2. In addition, the presence of sillimanite in some aggregates may be the result of back-reaction with

garnet + liquid + K-feldspar →

biotite + sillimanite + quartz

[reaction (R2) in the opposite sense], or may be produced by the reaction:

garnet + K-feldspar + $H_2O$ → sillimanite

+ biotite + quartz. (R7)

Both reaction (R6) and reaction (R7) require $H_2O$ as a reactant, which may come from crystallizing melts during retrogression. Also, the late replacement of K-feldspar and biotite by Ms + Qtz aggregates, the local growth of andalusite and the late S2 mylonitic fabrics formed under greenschist facies conditions indica r stages of the *P–T* path (Fig. 6).

The *P–T* evolution of the Lower Unit can be complemented by information from mineral assemblages formed during the D3 and D4 episodes of deformation. In the metapelites, development of syn-D3 Ms + Chl + Bt assemblages and replacement of garnet by Chl + Ms + Bt aggregates in syn-D4 shear-band planes suggests temperatures between 400 and 450 °C, which must have decreased progressively as indicated by the subsequent formation of normal ductile–brittle shear zones.

## THERMOBAROMETRY

### Mineral chemistry

Twelve samples of metapelite and felsic orthogneiss were selected for microprobe analysis of minerals of thermobarometric interest associated with the S2 fabrics. These samples come from scantily migmatized sectors of the upper and lower structural levels of the Lower Unit. Analyses were performed on a CAMECA electron microprobe in ED mode at Memorial University, Newfoundland (Canada), with erating potential, 50–75 s counting time, 20 nA specimen current and 1 μm beam diameter, except for plagioclase, for which a 10 nA specimen current and 5 μm beam diameter were used to avoid loss of Na. Data were reduced by a ZAF correction program. Structural formulae of minerals were calculated using the [illegible]4 software (unpublished software of J. Martignole and co-workers, Université de Montréal). Tables 1–5 give typical analyses of phases from three representative samples, 51-B and 51-T from the metapelites and 109-1 from the felsic orthogneisses.

#### *Garnet*

Analysed garnets grains are idiomorphic, with diameters of 4–6 mm. Analyses were performed along rim core–rim sections in order to detect chemical zoning. All garnet grains are characterized by chemically homogeneous cores and concentrically zoned outer sectors, whose width varies between 50 and 300 μm (Figs 7 & 8). Zoning is also observed around pull-aparts and biotite inclusions. Zoning is mainly expressed as an outward decrease of $X_{Mn}$ and, to a

th

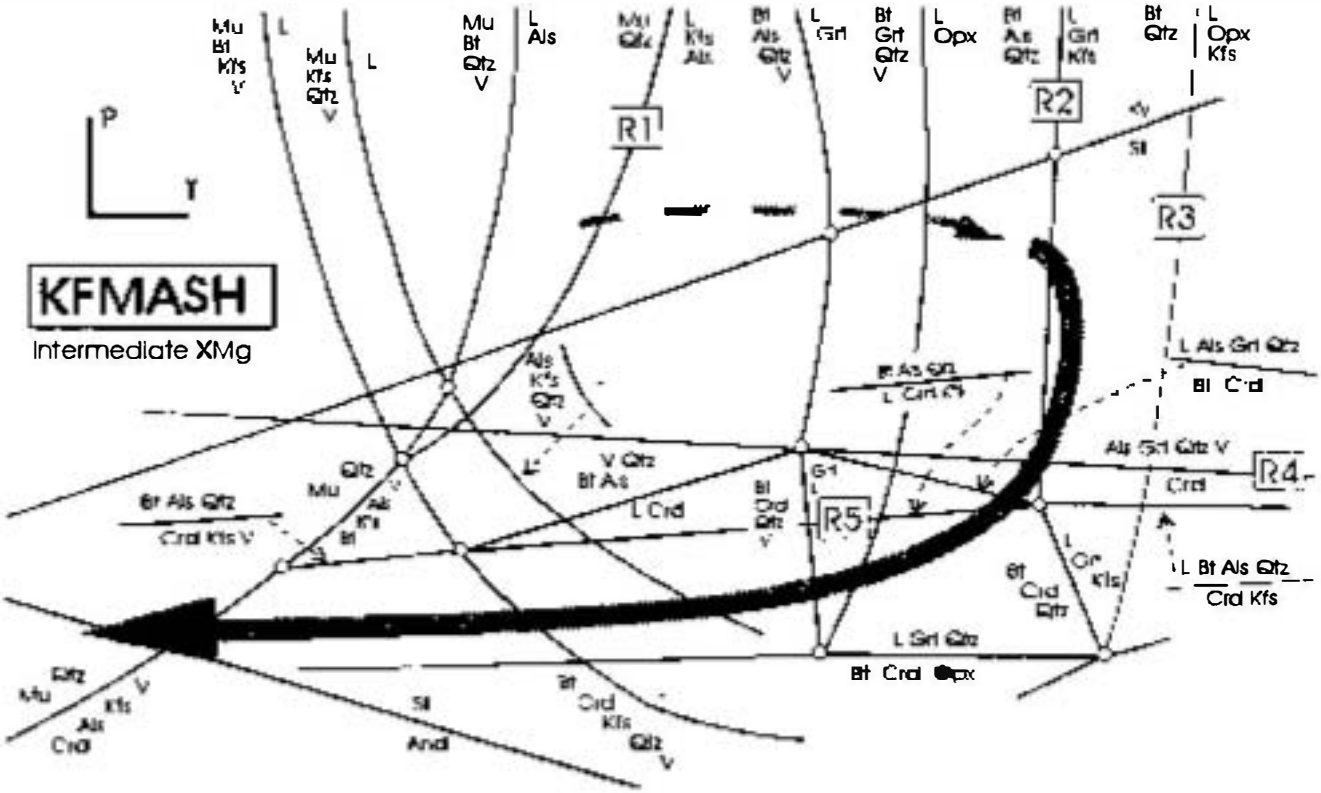


**Fig. 6.** Partial petrogenetic grid, based on the study by Vielzeuf & Holloway (1988), for metapelites with intermediate $X_{Mg}$ compositions. The KFMASH reactions shown are divariant fields, represented as lines for the sake of clarity. The arrow represents the *P–T* path inferred from the sequence of melting reactions and replacement microtextures shown by the Lower Unit during the D2 extensional event. $Al_2SiO_5$ triple point from Berman's (1991, updated to 1992) database.

**Table 1.** Representative garnet analyses from metapelitic gneisses. SAMPLE: sample number; POINT: analysis number in the profile; TYPE: c, analysis of the core zone; r, analysis of the rim zone; ct, analysis of biotite or plagioclase in contact with garnet; m, analysis of biotite in the matrix ('infinite reservoir'); #, analysis of biotite included in garnet. Each analysis is expressed as oxide in wt%, number of cations on the basis of 12 O for garnet, 11 O for biotite, 8 O for plagioclase and 3 O for ilmenite, and molar fractions; in ilmenite, molar fractions were calculated with the method of Rumble (1973).

| SAMPLE | 51-B | 51-B | 51-B | 51-B | 51-B | 51-B | 51-B | 51-B | 51-B | 51-T | 51-T | 51-T | 51-T | 51-T |
|---|---|---|---|---|---|---|---|---|---|---|---|---|---|---|
| POINT | 10-CD | 12-CD | 13-CD | 14-CD | 14-CDb | 01-AB | 01-CD | 01-CDb | 15-EF | 20-AB | 40-AB | 43-AB | 02-AB | 56-AB |
| TYPE | c | r | r | c | c | r | r | r | r | c | c | r | r | r |
| $SiO_2$ | 37.87 | 38.02 | 37.45 | 37.57 | 37.90 | 36.10 | 37.58 | 37.90 | 37.74 | 37.11 | 37.54 | 37.36 | 37.25 | 37.40 |
| $TiO_2$ | 0.00 | 0.00 | 0.00 | 0.09 | 0.01 | 0.03 | 0.11 | 0.07 | 0.12 | 0.01 | 0.15 | 0.11 | 0.03 | 0.01 |
| $Al_2O_3$ | 21.07 | 21.39 | 21.30 | 21.12 | 20.97 | 21.38 | 20.94 | 21.10 | 21.38 | 21.58 | 21.26 | 21.01 | 20.64 | 21.21 |
| FeO | 33.29 | 32.29 | 32.08 | 31.47 | 31.85 | 28.48 | 34.16 | 34.27 | 34.30 | 34.94 | 34.03 | 32.13 | 29.68 | 28.55 |
| MgO | 3.46 | 3.52 | 3.39 | 3.36 | 3.33 | 1.86 | 3.25 | 3.21 | 3.22 | 3.35 | 3.41 | 3.31 | 3.05 | 2.53 |
| MnO | 3.77 | 4.98 | 5.41 | 6.17 | 5.84 | 13.11 | 3.73 | 3.33 | 2.95 | 3.25 | 3.69 | 4.70 | 8.49 | 9.82 |
| CaO | 1.32 | 1.32 | 1.23 | 1.35 | 1.31 | 0.79 | 1.31 | 1.28 | 1.35 | 1.66 | 1.46 | 1.35 | 1.05 | 1.24 |
| Σ | 100.78 | 101.52 | 100.86 | 101.13 | 101.21 | 101.75 | 101.08 | 101.16 | 101.06 | 101.90 | 101.54 | 99.97 | 100.19 | 100.76 |
| Si | 3.02 | 3.01 | 2.99 | 2.99 | 3.02 | 3.00 | 3.00 | 3.02 | 3.00 | 2.99 | 3.00 | 3.00 | 3.00 | 3.00 |
| Ti | 0.00 | 0.00 | 0.00 | 0.01 | 0.00 | 0.00 | 0.01 | 0.00 | 0.01 | 0.00 | 0.01 | 0.00 | 0.00 | 0.00 |
| Al | 1.98 | 1.99 | 2.00 | 1.98 | 1.97 | 1.98 | 1.97 | 1.98 | 2.00 | 1.99 | 1.97 | 2.00 | 1.97 | 2.01 |
| $Fe^{2+}$ | 2.22 | 2.14 | 2.14 | 2.10 | 2.12 | 1.87 | 2.28 | 2.28 | 2.28 | 2.29 | 2.24 | 2.13 | 2.01 | 1.92 |
| Mg | 0.41 | 0.42 | 0.40 | 0.40 | 0.39 | 0.22 | 0.39 | 0.38 | 0.38 | 0.39 | 0.40 | 0.36 | 0.37 | 0.30 |
| Mn | 0.25 | 0.33 | 0.37 | 0.42 | 0.39 | 0.87 | 0.25 | 0.22 | 0.20 | 0.22 | 0.27 | 0.38 | 0.58 | 0.67 |
| Ca | 0.11 | 0.11 | 0.11 | 0.12 | 0.11 | 0.07 | 0.11 | 0.11 | 0.11 | 0.14 | 0.12 | 0.11 | 0.09 | 0.11 |
| Σ | 8.00 | 8.00 | 8.01 | 8.01 | 8.00 | 8.01 | 8.01 | 7.99 | 7.99 | 8.02 | 8.00 | 7.99 | 8.02 | 8.00 |
| $X_{Alm}$ | 0.74 | 0.71 | 0.71 | 0.69 | 0.70 | 0.62 | 0.75 | 0.76 | 0.77 | 0.75 | 0.74 | 0.72 | 0.65 | 0.64 |
| $X_{Prp}$ | 0.14 | 0.14 | 0.13 | 0.13 | 0.13 | 0.07 | 0.13 | 0.13 | 0.13 | 0.13 | 0.13 | 0.13 | 0.12 | 0.10 |
| $X_{Grs}$ | 0.04 | 0.04 | 0.04 | 0.04 | 0.04 | 0.02 | 0.04 | 0.04 | 0.04 | 0.05 | 0.04 | 0.04 | 0.03 | 0.04 |
| $X_{Sps}$ | 0.09 | 0.11 | 0.12 | 0.14 | 0.13 | 0.29 | 0.08 | 0.08 | 0.07 | 0.07 | 0.09 | 0.11 | 0.19 | 0.22 |
| $X_{Fe}$ | 0.84 | 0.84 | 0.84 | 0.84 | 0.84 | 0.89 | 0.85 | 0.86 | 0.86 | 0.85 | 0.85 | 0.84 | 0.84 | 0.86 |

**Table 2.** Representative garnet analyses from felsic orthogneisses. See Table 1 for details.

| SAMPLE | 109-1 | 109-1 | 109-1 | 109-1 | 109-1 | 109-1 | 109-1 |
|---|---|---|---|---|---|---|---|
| POINT | 34-AB | 40-AB | 40-ABb | 30-CD | 01-AB | 50-AB | 01-CD |
| TYPE | r | c | r | c | r | r | r |
| $SiO_2$ | 37.71 | 36.40 | 37.59 | 37.80 | 36.91 | 36.76 | 37.37 |
| $TiO_2$ | 0.01 | 0.15 | 0.12 | 0.05 | 0.05 | 0.13 | 0.01 |
| $Al_2O_3$ | 21.19 | 21.28 | 20.98 | 21.23 | 21.08 | 21.32 | 21.11 |
| FeO | 33.38 | 32.40 | 33.35 | 32.98 | 27.52 | 29.72 | 27.62 |
| MgO | 3.78 | 3.78 | 3.68 | 3.72 | 2.48 | 2.89 | 2.27 |
| MnO | 4.31 | 4.09 | 4.14 | 4.14 | 10.72 | 9.57 | 12.08 |
| CaO | 1.14 | 1.19 | 1.08 | 1.16 | 0.98 | 1.19 | 1.01 |
| Σ | 101.52 | 99.29 | 100.94 | 101.08 | 99.74 | 101.58 | 101.47 |
| Si | 2.99 | 2.95 | 3.00 | 3.00 | 2.99 | 2.98 | 2.99 |
| Ti | 0.00 | 0.01 | 0.01 | 0.00 | 0.00 | 0.01 | 0.00 |
| Al | 1.98 | 2.03 | 1.97 | 1.99 | 2.01 | 1.99 | 1.99 |
| $Fe^{2+}$ | 2.21 | 2.20 | 2.22 | 2.19 | 1.87 | 1.96 | 1.85 |
| Mg | 0.45 | 0.46 | 0.44 | 0.44 | 0.30 | 0.34 | 0.27 |
| Mn | 0.29 | 0.28 | 0.28 | 0.28 | 0.74 | 0.64 | 0.82 |
| Ca | 0.10 | 0.10 | 0.09 | 0.10 | 0.08 | 0.10 | 0.09 |
| Σ | 8.02 | 8.03 | 8.01 | 8.00 | 8.00 | 8.02 | 8.01 |
| $X_{Alm}$ | 0.72 | 0.72 | 0.73 | 0.73 | 0.62 | 0.64 | 0.61 |
| $X_{Prp}$ | 0.15 | 0.15 | 0.15 | 0.15 | 0.10 | 0.11 | 0.09 |
| $X_{Grs}$ | 0.03 | 0.03 | 0.03 | 0.03 | 0.03 | 0.03 | 0.03 |
| $X_{Sps}$ | 0.10 | 0.09 | 0.09 | 0.09 | 0.25 | 0.21 | 0.27 |
| $X_{Fe}$ | 0.83 | 0.83 | 0.83 | 0.83 | 0.86 | 0.85 | 0.87 |

minor extent, $X_{Prp}$, with the Fe/(Fe+Mg) ratio slightly increasing. There is also a marked outward increase of $X_{Sps}$, and $X_{Grs}$ is constant or decreases slightly in the outer 50 $\mu$m. Zoning is more pronounced towards Bt+Qtz±Pl aggregates that are products of garnet resorption (Figs 5f & 7b), at crystal rims or in fractures and pull-aparts. $X_{Alm}$ and $X_{Prp}$ also decrease towards biotite inclusions. Flat zoning profiles in the interiors of individual grains suggest compositional homogenization by diffusion at high temperatures. On the other hand, trends of the rim zoning are typical of retrogression. Given the textural evidence of retrograde consumption of garnet, they most likely resulted from a combination of net transfer reactions and Fe–Mg exchange between garnet and biotite (Spear, 1989).

### *Biotite*

In both the metapelites and the felsic orthogneisses, three types of biotite have been distinguished in terms of microtextural setting: biotite touching garnet or included in it (type 1); biotite adjacent to, but not in contact with the garnet, located in the garnet resorption microdomains (type 2); and matrix biotite away from garnet (type 3). These three types of biotite have distinct compositions in terms of Fe and Mg. In the metapelites, Fe/(Fe+Mg) ratios range between 0.58 and 0.59, and 0.60 and 0.66 for types 1 and 2, respectively, whereas in the felsic orthogneisses these ratios vary between 0.61 and 0.69, and 0.60 and 0.73. Type 1 biotite is slightly zoned, with Fe/(Fe+Mg) increasing towards the contact with garnet. Type 2 biotite displays a decrease in the Fe/(Fe+Mg) ratio with increasing distance from garnet. Matrix (type 3) biotite is statistically the most abundant and is chemically homogeneous with Fe/(Fe+Mg) ratios between 0.58 and 0.60. Therefore, overall variations in Fe/(Fe+Mg) in biotite depend upon the textural relationship with garnet. With increasing distance from garnet these ratios first increase from type 1 to type 2 biotite, then decrease within type 2 and display minimum values in type 3 biotite (Fig. 9a). All types of biotite are characterized by variable Ti contents with $X_{Ti}$ in octahedral sites ranging from 0.1 to 0.24

**Table 3.** Representative analyses of biotite. See Table 1 for details.

| SAMPLE | 51-B | 51-B | 51-B | 51-T | 51-T | 51-T | 109-1 | 109-1 | 109-1 | 109-1 | 109-1 |
|---|---|---|---|---|---|---|---|---|---|---|---|
| POINT | BT-8 | Bt-9 | Bt-11 | BT-4 | BT-5 | BT-1 | BT-6 | BT-7 | Bt-11 | Bt-4 | Bt-2 |
| TYPE | m | m | m | m | m | ct | m | m | m | ct | # |
| $SiO_2$ | 35.88 | 35.81 | 36.08 | 35.16 | 35.84 | 35.35 | 35.63 | 35.67 | 35.35 | 35.39 | 35.61 |
| $TiO_2$ | 3.20 | 3.83 | 3.60 | 3.55 | 3.68 | 3.35 | 3.73 | 3.55 | 2.50 | 3.85 | 3.72 |
| $Al_2O_3$ | 20.41 | 20.14 | 19.97 | 19.44 | 19.96 | 19.15 | 19.44 | 19.89 | 19.12 | 19.00 | 19.44 |
| FeO | 20.28 | 20.18 | 20.51 | 20.41 | 19.85 | 21.54 | 20.29 | 20.05 | 21.35 | 20.24 | 20.62 |
| MgO | 8.08 | 8.17 | 7.79 | 7.43 | 7.32 | 7.43 | 7.60 | 7.83 | 8.07 | 7.83 | 7.17 |
| MnO | 0.34 | 0.34 | 0.38 | 0.39 | 0.45 | 0.52 | 0.38 | 0.49 | 0.45 | 0.48 | 0.62 |
| CaO | 0.03 | 0.00 | 0.07 | 0.00 | 0.00 | 0.02 | 0.02 | 0.07 | 0.05 | 0.02 | 0.03 |
| $Na_2O$ | 0.42 | 0.37 | 0.29 | 0.41 | 0.23 | 0.03 | 0.27 | 0.25 | 0.27 | 0.23 | 0.12 |
| $K_2O$ | 9.60 | 9.86 | 9.49 | 9.54 | 9.57 | 9.39 | 9.56 | 9.54 | 9.59 | 9.67 | 9.54 |
| Σ | 98.24 | 98.70 | 98.18 | 96.33 | 96.90 | 96.78 | 96.92 | 97.34 | 96.75 | 96.71 | 96.87 |
| Si | 2.66 | 2.64 | 2.68 | 2.67 | 2.69 | 2.68 | 2.68 | 2.67 | 2.68 | 2.67 | 2.69 |
| Ti | 0.18 | 0.21 | 0.20 | 0.20 | 0.21 | 0.19 | 0.21 | 0.20 | 0.14 | 0.22 | 0.21 |
| $Al^{IV}$ | 1.34 | 1.36 | 1.33 | 1.33 | 1.31 | 1.32 | 1.32 | 1.33 | 1.32 | 1.33 | 1.31 |
| $Al^{VI}$ | 0.44 | 0.40 | 0.42 | 0.41 | 0.45 | 0.39 | 0.41 | 0.42 | 0.39 | 0.37 | 0.41 |
| $Fe^{2+}$ | 1.26 | 1.25 | 1.27 | 1.29 | 1.24 | 1.36 | 1.28 | 1.25 | 1.35 | 1.28 | 1.30 |
| Mg | 0.89 | 0.90 | 0.86 | 0.84 | 0.82 | 0.84 | 0.85 | 0.87 | 0.91 | 0.88 | 0.81 |
| Mn | 0.02 | 0.02 | 0.02 | 0.03 | 0.03 | 0.03 | 0.02 | 0.03 | 0.03 | 0.03 | 0.04 |
| Oct. | 2.79 | 2.78 | 2.78 | 2.77 | 2.75 | 2.82 | 2.77 | 2.78 | 2.83 | 2.78 | 2.77 |
| Ca | 0.00 | 0.00 | 0.01 | 0.00 | 0.00 | 0.00 | 0.00 | 0.01 | 0.00 | 0.00 | 0.00 |
| Na | 0.06 | 0.05 | 0.04 | 0.06 | 0.03 | 0.00 | 0.04 | 0.04 | 0.04 | 0.03 | 0.02 |
| K | 0.91 | 0.93 | 0.90 | 0.92 | 0.92 | 0.91 | 0.92 | 0.91 | 0.93 | 0.93 | 0.92 |
| Alk. | 0.97 | 0.98 | 0.94 | 0.98 | 0.95 | 0.91 | 0.95 | 0.95 | 0.97 | 0.97 | 0.94 |
| $X_{Phl}$ | 0.32 | 0.32 | 0.31 | 0.30 | 0.30 | 0.30 | 0.31 | 0.31 | 0.32 | 0.32 | 0.29 |
| $X_{Ann}$ | 0.45 | 0.45 | 0.46 | 0.47 | 0.45 | 0.48 | 0.46 | 0.45 | 0.48 | 0.46 | 0.47 |
| $X_{Fe}$ | 0.58 | 0.58 | 0.60 | 0.59 | 0.60 | 0.62 | 0.60 | 0.59 | 0.60 | 0.61 | 0.62 |

**Table 4** Representative plagioclase analyses. See Table 1 for details.

| SAMPLE | 51–Bc | 51–B | 51–B | 51–B | 51–B | 51–T | 51–T | 51–T | 51–T | 109-1 | 109-1 | 109-1 | 109-1 | 109-1 |
|---|---|---|---|---|---|---|---|---|---|---|---|---|---|---|
| POINT | Pl–5 | Pl–30 | Pl–2 | Pl–32 | Pl–44 | Pl–1 | Pl–4 | Pl–4 | Pl–28 | Pl–1C | Pl–3C | PL–9 | Pl–2B | Pl–8B |
| TYPE | | | | | ct | | | | | | | | | |
| $SiO_2$ | 60.91 | 61.46 | 63.47 | 63.19 | 61.15 | 64.06 | 64.69 | 61.53 | 61.25 | 64.06 | 64.12 | 64.39 | 63.87 | 64.02 |
| $Al_2O_3$ | 25.44 | 25.67 | 23.70 | 23.53 | 24.93 | 23.11 | 22.05 | 25.25 | 25.00 | 23.11 | 23.18 | 23.29 | 23.51 | 23.27 |
| FeO | 0.00 | 0.05 | 0.12 | 0.13 | 0.00 | 0.06 | 0.00 | 0.08 | 0.04 | 0.06 | 0.01 | 0.18 | 0.02 | 0.03 |
| CaO | 6.50 | 6.41 | 4.38 | 4.58 | 6.46 | 3.93 | 3.79 | 6.49 | 6.41 | 3.93 | 4.30 | 4.13 | 4.75 | 4.45 |
| $Na_2O$ | 8.27 | 7.65 | 9.33 | 8.93 | 7.98 | 9.50 | 9.58 | 8.15 | 8.25 | 9.50 | 9.00 | 9.27 | 9.13 | 9.10 |
| $K_2O$ | 0.21 | 0.24 | 0.14 | 0.06 | 0.27 | 0.13 | 0.05 | 0.16 | 0.14 | 0.13 | 0.05 | 0.28 | 0.21 | 0.24 |
| Σ | 101.33 | 101.48 | 101.14 | 100.42 | 100.79 | 100.79 | 100.16 | 101.66 | 101.09 | 100.79 | 100.66 | 101.54 | 101.49 | 101.11 |
| | 2.68 | 2.69 | 2.78 | 2.79 | 2.70 | 2.81 | 2.85 | 2.69 | 2.70 | 2.81 | 2.81 | 2.80 | 2.79 | 2.80 |
| | 1.32 | 1.32 | 1.22 | 1.22 | 1.30 | 1.19 | 1.16 | 1.30 | 1.30 | 1.19 | 1.20 | 1.20 | 1.21 | 1.20 |
| | 0.00 | 0.00 | 0.00 | 0.00 | 0.00 | 0.00 | 0.00 | 0.00 | 0.00 | 0.00 | 0.00 | 0.01 | 0.00 | 0.00 |
| | 3.99 | 4.02 | 4.01 | 4.01 | 4.00 | 4.01 | 4.01 | 4.00 | 4.00 | 4.01 | 4.01 | 4.01 | 4.00 | 4.00 |
| Ca | 0.31 | 0.30 | 0.21 | 0.22 | 0.31 | 0.18 | 0.18 | 0.30 | 0.30 | 0.18 | 0.20 | 0.19 | 0.22 | 0.21 |
| Na | 0.70 | 0.65 | 0.79 | 0.76 | 0.68 | 0.81 | 0.82 | 0.69 | 0.70 | 0.81 | 0.77 | 0.78 | 0.77 | 0.77 |
| K | 0.01 | 0.01 | 0.01 | 0.00 | 0.02 | 0.01 | 0.00 | 0.01 | 0.01 | 0.01 | 0.00 | 0.02 | 0.01 | 0.01 |
| Alk. | 1.02 | 0.96 | 1.01 | 0.98 | 1.00 | 1.00 | 1.00 | 1.00 | 1.01 | 1.00 | 0.97 | 0.99 | 1.01 | 0.99 |
| | 0.69 | 0.67 | 0.79 | 0.78 | 0.68 | 0.81 | 0.82 | 0.69 | 0.69 | 0.81 | 0.79 | 0.79 | 0.77 | 0.78 |
| | 0.30 | 0.31 | 0.20 | 0.22 | 0.30 | 0.18 | 0.18 | 0.30 | 0.30 | 0.18 | 0.21 | 0.19 | 0.22 | 0.21 |
| | 0.01 | 0.01 | 0.01 | 0.00 | 0.02 | 0.01 | 0.00 | 0.01 | 0.01 | 0.01 | 0.00 | 0.02 | 0.12 | 0.01 |

**Table 5** Representative ilmenite analyses (cationic content). See Table 1 for details.

| SAMPLE | 51–B | 51–B | 51–B | 51–T | 51–T | 51–T | 109–1 | 109–1 |
|---|---|---|---|---|---|---|---|---|
| POINT | ilm–2 | ilm–14 | ilm–17 | ilm–1 | ilm–4 | ilm–7 | ilm–4 | ilm–12 |
| Ti | 1.01 | 1.01 | 1.01 | 1.01 | 1.01 | 1.01 | 1.01 | 1.02 |
| $Fe^{2+}$ | 0.80 | 0.88 | 0.78 | 0.88 | 0.81 | 0.89 | 0.81 | 0.82 |
| Mn | 0.19 | 0.08 | 0.16 | 0.08 | 0.16 | 0.06 | 0.15 | 0.13 |
| $X_{Fe_2O_3}$ | 0.01 | 0.01 | 0.01 | 0.00 | 0.01 | 0.00 | 0.02 | 0.00 |
| $X_{FeTiO_3}$ | 0.97 | 0.96 | 0.96 | 0.96 | 0.91 | 0.97 | 0.97 | 0.96 |
| $X_{MnTiO_3}$ | 0.01 | 0.03 | 0.03 | 0.04 | 0.08 | 0.03 | 0.01 | 0.04 |

(Fig. 9b). Biotite with low Ti contents also shows exsolution of ilmenite ± rutile, a common retrogression feature in high-grade rocks (Spear *et al.*, 1990; Fig. 9b).

### *Plagioclase*

Plagioclase compositions range between $An_{10}$ and $An_{32}$ in the metapelites and $An_{15}$ and $An_{30}$ in the felsic orthogneisses (Fig. 10a). Two textural types are distinguished: matrix plagioclase and plagioclase in contact with garnet. Matrix plagioclase forms millimetric porphyroblasts, elongated along the S2 fabric, and displays the highest anorthite contents ($An_{22-32}$). These crystals are chemically homogeneous ($An_{29-31}$ in metapelites and $An_{26-30}$ in felsic orthogneisses) or display normal zoning (Fig. 10c), but locally smaller grains with inverse zoning ($An_{22-30}$ and $An_{27-29}$) also occur. The porphyroblasts are locally rimmed by small recrystallized plagioclase crystals, with irregular outlines, which are less anorthitic ($An_{20-24}$). Grains close to, or in contact with garnet and not in the resorption zones are subidiomorphic and show normal zoning ($An_{29-12}$ or $An_{30-12}$) with lowest anorthite contents close to the garnet (Fig. 10b). They are locally rimmed by small recrystallized plagioclase in contact with the garnet, of a less anorthitic composition ($An_{12-18}$).

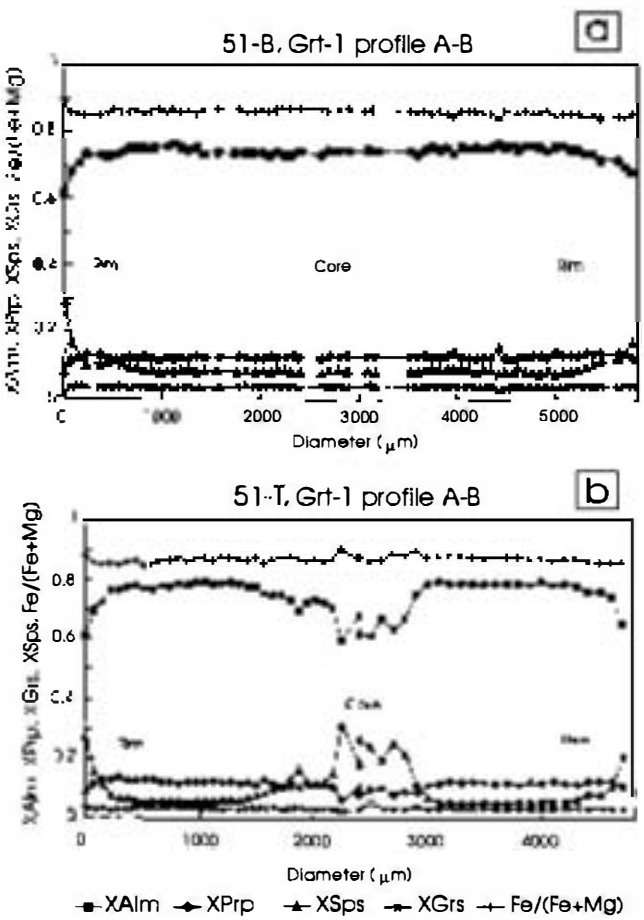


**Fig. 7.** Chemical profiles of garnet in metapelites of the Lower Unit.

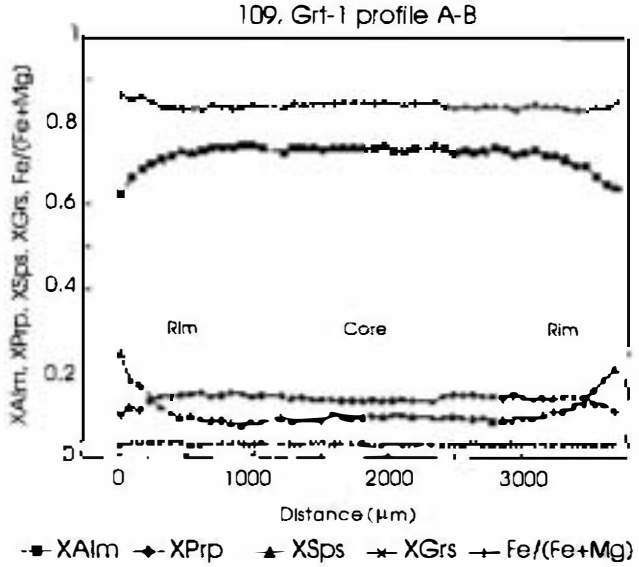


**Fig. 8.** Chemical profiles of garnet in felsic orthogneisses of the Lower Unit.

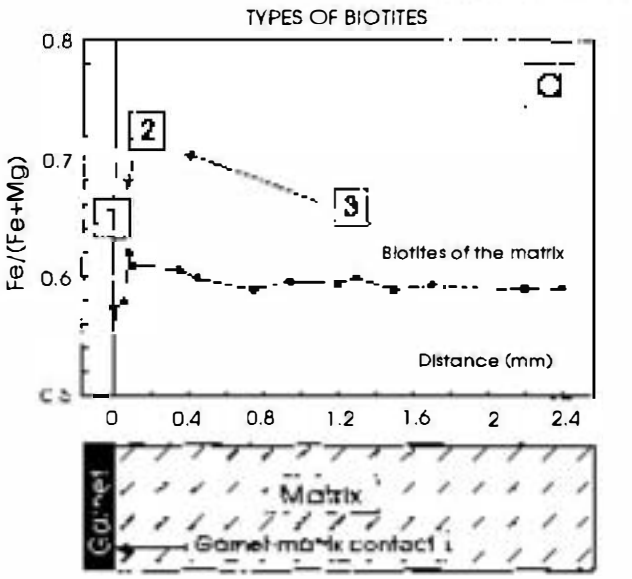


Grains in zones of garnet resorption display inverse zoning, with $An_{18-30}$ in metapelites and $(An_{27-32})$ in the felsic orthogneisses (Fig. 10d).

*Fe–Ti oxides*

Fe–Ti oxides occur as inclusions in garnet, in syn-S2 sillimanite and in K-feldspar porphyroblasts, and are considered to belong to the peak mineral assemblage. They were analysed to gain information on the partial pressure of oxygen and to allow estimation of $Fe^{3+}$ in biotite, which cannot be obtained by microprobe analysis. Analysed grains appear fresh and, as shown by SEM images, devoid of exsolution microtextures. In both the metapelites and the felsic orthogneisses, the composition of the Fe–Ti oxides is close to pure ilmenite, with negligible $X_{Fe_2O_3}$ (Fig. 11a). These values indicate low $f_{O_2}$ conditions at the metamorphic peak, in the stability field of the magnetite, that is below the HM buffer and above the QFM buffer, with $f_{O_2}$ values between $10^{-11}$ and $10^{-17}$ bar, for the range 700–750 °C (Ernst, 1976; in Spear, 1993). According to the empirical correlation between the $X_{Fe_2O_3}$ in ilmenite and the $Fe^{3+}/(Fe^{3+}+Fe^{2+})$ ratio in coexisting biotite established by Williams & Grambling (1990), $X_{Fe_2O_3} \approx 0$ in ilmenite corresponds to $Fe^{3+}/(Fe^{3+}+Fe^{2+}) \approx 0.12$ in biotite, which is considered to be the minimum $Fe^{3+}$ content in natural biotite (Fig. 11b).

*Interpretation*

The observed zoning trends in garnet and plagioclase and the compositional variations in biotite can be interpreted in terms of reactions, most of which operated during retrogression. The outward increase in the Fe/(Fe+Mg) ratio of garnet is consistent with

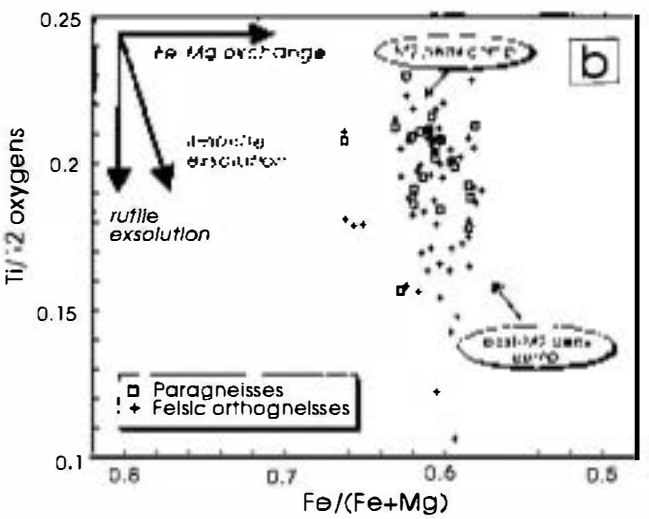


**Fig. 9.** Compositional variation of biotite expressed by (a) the Fe/(Fe+Mg) ratio according to variable distance from garnet rim, and (b) the substitution of Ti in octahedral positions (see text for explanation).

both Fe–Mg exchange between garnet and biotite during cooling, and net transfer reactions, leading to biotite production at the expense of the Fe–Mg components in garnet, such as reactions (R6) and (R7), which are responsible for the development of the retrograde $Bt \pm Pl \pm Sil - Qtz$ aggregates. The $X_{Grs}$ decrease is consistent with grossular consumption by reaction (R6) or by the GASP reaction,

$$Ca_3Al_2Si_3O_{12} + 2Al_2SiO_5 + SiO_2 \rightarrow 3CaAl_2Si_2O_8. \quad \text{(GASP)}$$

Both reactions have a positive slope in $P$–$T$ space, with grossular being consumed on the low-pressure

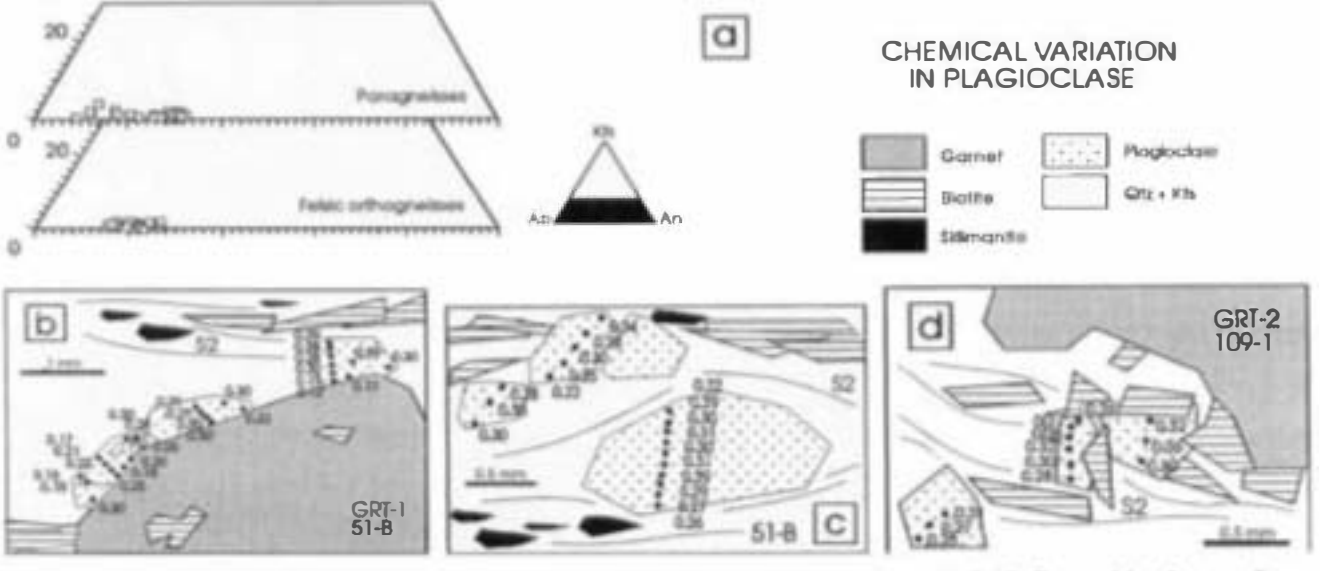


**Fig. 10.** (a) Compositional variation of plagioclase in the An–Ab–Kfs triangular diagram. (b), (c) & (d) Compositional types of plagioclase according to zoning and textural position (see text for explanation).

side, hence the outward decrease of $X_{Grs}$ in garnet is compatible with a decrease in pressure during retrogression. The rimward increase in $X_{Sps}$ is the consequence of garnet consumption reactions, since Mn is not an essential component of any phase of the matrix.

The dominance of net transfer reactions such as reactions (R6) and (R7) over the Fe–Mg exchange reaction results in an increase of Fe/(Fe + Mg) in biotite (Spear & Florence, 1992), which accounts for the Fe enrichment in type 2 biotite. On the other hand, the decrease in the Fe/(Fe + Mg) from type 2 to type 1 biotite indicates that the net transfer reactions were arrested before the exchange reaction, making the garnet richer in Fe and the biotite richer in Mg.

During progressive metamorphism in pelitic systems, the grossular component in garnet forms at the expense of anorthite, plagioclase thus becoming more albitic, provided that no other calcic phases exist in the mineral assemblage and that the system remained closed to Na and Ca (Spear *et al.*, 1991). In this context, the observed normal zoning in large matrix plagioclase and in grains with straight contacts against idioblastic garnet (Fig. 10b & c) is interpreted as a prograde feature, and the most albitic compositions, that is those of the rims and of the recrystallized grains surrounding the large crystals, are interpreted as representative of the metamorphic peak. On the other hand, the inversely zoned plagioclase can only be related to anorthite production at the expense of grossular during retrogression (see above).

#### Selection of analyses

By applying thermobarometry to suitable mineral assemblages that contain garnet with diffusion-controlled zoning, it is possible to determine two points on the $P$–$T$ path, one corresponding to the thermal peak and one corresponding to the closure of the retrograde reactions (Spear, 1989; Anovitz & Essene, 1990). This is the only information that can be extracted from rocks such as those of the Lower Unit of the TGD, since homogenization of garnet at high temperatures has erased its prograde history. However, this approach is based upon two major assumptions: (1) that the mineral compositions acquired at the thermal peak have been preserved and can be recognized; and (2) that retrograde reactions responsible for the composition of the rims all ceased at the same time.

The extent to which the homogenized core of garnet maintains the composition achieved during the thermal peak depends upon the size of the garnet, the peak temperature and the cooling rate (Spear, 1991). As a general rule, large garnet grains (i.e. several millimetres in diameter) have more chance of preserving peak compositions. Moreover, the relatively rapid cooling of the Lower Unit at exhumation rates of $\approx 2$ mm/year (Escuder Viruete *et al.*, 1994) suggests that diffusion at the grain scale during cooling was of minor importance in the rocks studied.

On the other hand, relatively rapid diffusion in biotite means that compositional changes occur at the grain scale even during retrogression. The effect of this can be minimized if biotite is much more abundant than garnet (infinite reservoir concept, Spear, 1991) and if matrix biotite away from garnet is used, so that changes in $P$–$T$ conditions responsible for the retrograde zoning in garnet would not have significantly modified the composition of biotite. Samples used for this study have modal ratios of garnet over biotite of between 0.1 and 0.05, implying a situation close to an infinite reservoir. Finally, the interpretation of zoning

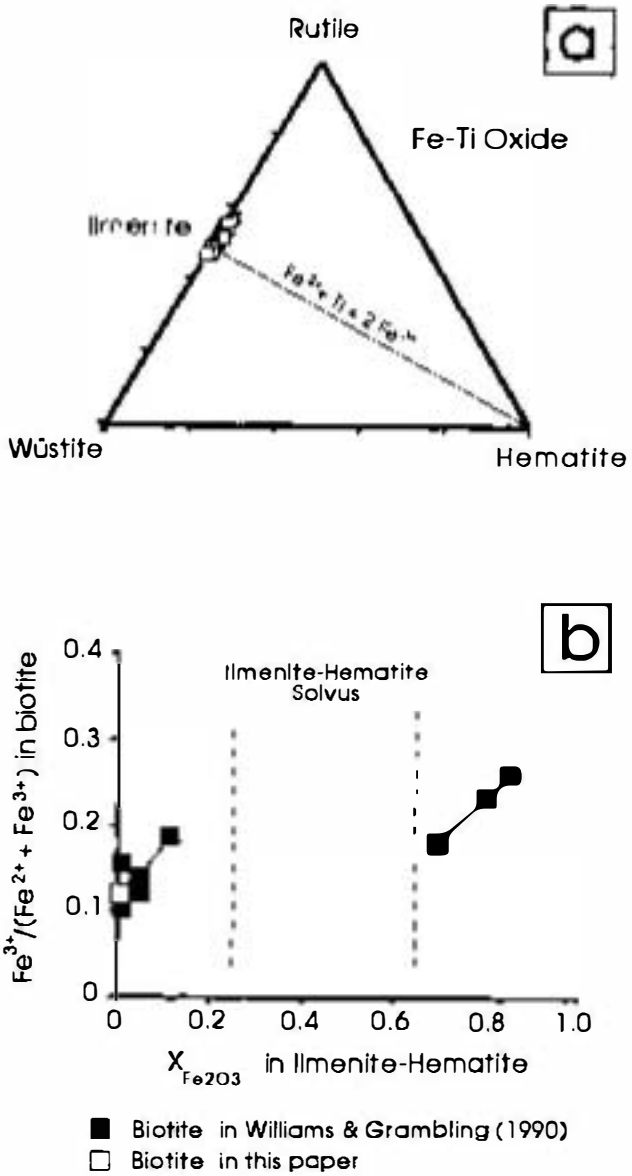


**Fig. 11.** (a) Composition of the Fe–Ti oxides. (b) Correlation proposed by Williams & Grambling (1990) between $X_{Fe_2O_3}$ in ilmenite and $Fe^{3+}/(Fe^{2+} + Fe^{3+})$ ratio in the biotite, and comparison with the biotite studied in this paper.

in plagioclase discussed in the previous section showed that only the rims of grains displaying normal zoning can be considered as representative of the thermal peak. Therefore, in the samples studied, the compositions of the homogeneous cores of the largest garnet grains (diameter 4–6 mm) were combined with the composition of type 3 biotite and with the rims of plagioclase with normal zoning in order to obtain $P$–$T$ conditions close to the thermal peak.

The second assumption, that of coeval closure of all reactions, is unlikely, since Fe–Mg exchange thermometers are known to close at lower temperatures than net-transfer barometric reactions (Frost & Chacko, 1989; Spear & Florence, 1992). However, retrograde $P$–$T$ conditions corresponding to the closure of the GASP net-transfer reaction can be calculated by using touching rims of garnet and plagioclase with reverse zoning and adjacent biotite, avoiding garnet rims touching biotite.

### Thermobarometric method

Both peak and retrograde $P$–$T$ conditions were calculated with the Bt–Grt thermometer and the GASP barometer using the TWEEQU software of Berman (1991, updated to 1992). This software uses an internally consistent thermodynamic database and incorporates appropriate activity models for non-ideal solid solutions (garnet: Berman, 1990; Berman & Koziol, 1991; biotite: McMullin *et al.*, 1991; plagioclase: Fuhrman & Lindsley, 1988; Aranovich & Podlesskii, 1989).

#### *Garnet–biotite thermometry in Mn-rich rocks*

A peculiar characteristic of some garnet in the felsic orthogneisses is high $X_{Sps}$ values, up to 0.30 at the rims and up to 0.12 at the cores. The activity model for garnet, incorporated in the TWEEQU software, considers ideal Fe–Mn, Mg–Mn and Ca–Mn mixing. This consideration seems to be adequate in rocks poor in Mn, but is open to question for Mn-rich garnet. Williams & Grambling (1990) proposed an empirical Grt–Bt thermometer (WG thermometer) for garnet rich in Mn, which considers a non-ideal Mn–Mg–Fe mixture in the garnet and assumes, in addition, non-ideal mixing for Ti, Al and $Fe^{3+}$ in the octahedral site in biotite. This thermometer was used for the calculation of the equilibrium temperatures with the cores and rims of spessartine-rich garnet in order to compare the results with the temperatures obtained by the TWEEQU method.

### Results and Interpretation

$P$–$T$ conditions obtained in metapelites of the upper structural levels of the Lower Unit (51-B and 51-T), and in felsic orthogneisses of the lower structural levels (109–1) are shown in Table 6. This table includes $P$–$T$ conditions calculated using the TWEEQU method with (1) the Aranovich & Podlesskii (1989) ($P_{AP}$–$T_{AP}$) and (2) the Fuhrman & Lindley (1989) ($P_{FL}$–$T_{FL}$) activity models for plagioclase. The former model assumes a subregular solution and was suggested by R. Berman (personal communication, 1994) to be valid for plagioclase with an An content below 20%, as in the samples used in this study, for which other widely used models fail. Indeed, $P_{FL}$–$T_{FL}$ values are 0.5–2 kbar higher than $P_{AP}$–$T_{AP}$ values , and in sample 51-T they fall within the kyanite stability field, which is not consistent with the mineral assemblage; therefore, they are considered as overestimates. Table 6 also gives temperatures at the intersection between the GASP

**Table 6** *P–T* results. SAMPLE: sample number and textural position of the analysis: c, core of garnet; r, rim of garnet; POINT: number of garnet analysis; $P_{FL}$–$T_{FL}$: *P–T* intersections obtained with the activity model of Fuhrman & Lindsley (1988) for plagioclase; $P_{AP}$–$T_{AP}$: *P–T* intersections calculated with the activity model of Aranovich & Podlesskii (1989) for plagioclase; $T_{WG}$: temperature obtained with the geothermometer of Williams & Grambling (1990); σ: standard deviation. Samples 51-B and 51-T: metapelites from the upper structural levels of the Lower Unit; sample 109-1: felsic orthogneisses of the lower structural levels of the Lower Unit. Pressure in kbar and temperature in °C.

| SAMPLE | POINT | $P_{FL}$ | $T_{FL}$ | $P_{AP}$ | $T_{AP}$ | $T_{WG}$ |
|---|---|---|---|---|---|---|
| 51–B, c | 12-AB | 6.78 | 724.9 | 5.69 | 718.8 | 743.9 |
| 51–B, c | 14-AB | 7.86 | 737 | 6.69 | 730.4 | 779.3 |
| 51–B, c | 14-ABb | 7.34 | 734.1 | 6.25 | 727.9 | 777.3 |
| 51–B, c | 15-AB | 7.65 | 725.6 | 6.52 | 723.8 | 776.8 |
| 51–B, c | 15-ABb | 7.14 | 722.8 | 6.06 | 716.7 | 776.5 |
| 51–B, c | 71-AB | 7.02 | 737.1 | 7.05 | 751.2 | 780.9 |
| 51–B, c | 02-CD | 6.75 | 702.9 | 5.63 | 696.6 | 694.2 |
| 51–B, c | 10-CD | 7.9 | 749.2 | 6.88 | 749.8 | 780.2 |
| 51–B, c | 10-CDb | 7.4 | 746.2 | 6.32 | 725.8 | 777.7 |
| 51–B, c | 12-CD | 7.7 | 761.1 | 6.57 | 754.5 | 775.7 |
| 51–B, c | 13-CD | 7.66 | 749.1 | 6.48 | 742.4 | 778.4 |
| 51–B, c | 14-CD | 8.25 | 758.1 | 7.05 | 751.2 | 780.9 |
| 51–B, c | 14-CDb | 7.72 | 755 | 6.61 | 748.4 | 778.9 |
| $\bar{x}$ | cores | 7.45 | 738.5 | 6.44 | 733.6 | 768.6 |
| | σ | ±0.42 | ±15.4 | ±0.43 | ±16.8 | ±24.4 |
| 51–B, r | 01-CD | 5.02 | 704.8 | 4.36 | 700.3 | 742.5 |
| 51–B, r | 01-CDb | 4.89 | 685.3 | 4.13 | 681.5 | 741.6 |
| 51–B, r | 01-AB | 4.34 | 669.2 | 3.7 | 665.6 | 739.7 |
| 51–B, r | 77-AB | 4.05 | 703.5 | 3.46 | 700.3 | 738.7 |
| 51–B, r | 15-EF | 4.42 | 669.6 | 3.76 | 665.9 | 718.4 |
| 51–B, r | 15-EFb | 4.72 | 684.3 | 4.05 | 680.8 | 719.6 |
| $\bar{x}$ | rims | 4.57 | 686.1 | 3.91 | 682.4 | 733.4 |
| | σ | ±0.33 | ±14.2 | ±0.29 | ±11.1 | ±10.3 |
| 51–T, c | 20-AB | 9.26 | 739.1 | 7.96 | 750.2 | 766.9 |
| 51–T, c | 37-AB | 8.64 | 736.3 | 7.37 | 729.1 | 732.1 |
| 51–T, c | 37-ABb | 9.75 | 751.5 | 8.39 | 744.6 | 736.3 |
| 51–T, c | 40-AB | 9.92 | 759.1 | 8.55 | 751.3 | 769.4 |
| 51–T, c | 40-ABb | 10.12 | 768.7 | 8.75 | 761.8 | 770.5 |
| 51–T, c | 43-AB | 8.82 | 756.5 | 7.52 | 749.1 | 764.9 |
| $\bar{x}$ | cores | 9.41 | 751.8 | 8.09 | 747.6 | 756.6 |
| | σ | ±0.55 | ±11.2 | ±0.51 | ±9.70 | ±16.0 |
| 51–T, r | 01-AB | 3.18 | 614.5 | 2.5 | 610.2 | 667.4 |
| 51–T, r | 02-AB | 4.5 | 730.2 | 3.72 | 725.6 | 782.7 |
| 51–T, r | 02-ABb | 4.28 | 738.2 | 3.46 | 724.4 | 723.2 |
| 51–T, r | 55-ABb | 4.08 | 677.8 | 3.43 | 661.4 | 723 |
| 51–T, r | 56-ABb | 4.12 | 665.5 | 3.49 | 660.8 | 723.2 |
| $\bar{x}$ | rims | 4.03 | 685.2 | 3.32 | 676.7 | 723.9 |
| | σ | ±0.45 | ±45.3 | ±0.42 | ±43.7 | ±36.4 |
| 109–1, c | 34-AB | 8.23 | 786.7 | 7.02 | 779.5 | 776.9 |
| 109–1, c | 40-AB | 8.88 | 781.9 | 7.51 | 774.2 | 809.8 |
| 109–1, c | 40-ABb | 9.22 | 800.2 | 7.81 | 792.2 | 811.2 |
| 109–1, c | 07-CD | 8.63 | 799.1 | 7.37 | 791.8 | 790.2 |
| 109–1, c | 27-CD | 8.08 | 757.6 | 6.76 | 750.2 | 769.3 |
| 109–1, c | 30-CD | 8.44 | 767.8 | 7.1 | 760.2 | 770.8 |
| 109–1, c | 40-CD | 7.91 | 776.3 | 6.76 | 769.7 | 806.3 |
| $\bar{x}$ | cores | 8.48 | 781.3 | 7.19 | 773.9 | 790.6 |
| | σ | ±0.42 | ±14.5 | ±0.36 | ±14.4 | ±17.2 |
| 109–1, r | 01-AB | 4.27 | 645.8 | 3.35 | 640.6 | 710.4 |
| 109–1, r | 50-AB | 5.8 | 690.1 | 4.82 | 684.5 | 742.3 |
| 109–1, r | 01-CD | 3.71 | 613.7 | 2.08 | 608.8 | 683.7 |
| $\bar{x}$ | rims | 4.59 | 649.8 | 3.41 | 644.6 | 712.1 |
| | σ | ±0.88 | ±31.3 | ±1.12 | ±31.1 | ±23.9 |

equilibrium and the WG thermometer ($T_{WG}$). *P–T* conditions obtained from the intersection between the GASP equilibria calculated with TWEEQU using the Aranovich & Podlesskii (1989) model and the Grt–Bt equilibria calculated with TWEEQU and the WG thermometer, and *P–T* vectors, are shown in Fig. 12, together with relevant reaction boundaries implied by textural and melting relationships.

The mean $T_{AP}$ values for the thermal peak obtained in the metapelites of the upper structural levels are 734 and 748 °C, slightly lower than those obtained in the felsic orthogneisses of the lower structural levels, which are 774 °C. Corresponding mean $P_{AP}$ values are 6.4 and 8.1 kbar for the upper structural levels, and 7.2 kbar for the lower levels. Retrograde *P–T* conditions overlap in the different structural levels. $T_{WG}$ values are higher than $T_{AP}$ by 5–40 °C for the thermal peak and 40–70 °C for the retrograde conditions, the latter difference being larger owing to the high Mn contents of the garnet rims. Consequently, pressure conditions corresponding to $T_{WG}$ are 0.2–1.4 kbar higher than those corresponding to $T_{AP}$ (Fig. 12), given the positive slope of the curve of the GASP barometer in *P–T* space.

*P–T* vectors between maximum and retrograde *P–T* conditions indicate decompression of 3–5 kbar combined with cooling of a few tens of degrees (Fig. 12), the steepest vectors corresponding to the upper levels (Fig. 12a & b). Since retrograde $T_{WG}$ values are higher than $T_{AP}$ conditions, $P_{WG}$–$T_{WG}$ vectors are steeper than $P_{AP}$–$T_{AP}$ vectors. These *P–T* vectors are consistent with textural evidence of decompression, and, since they are steeper than the GASP reaction following Frost & Chacko (1989), they are not an artefact related to the closing of the Fe–Mg exchange equilibrium between garnet and biotite at a lower temperature than the GASP equilibrium. The thermobarometric results also indicate that the felsic orthogneisses of the lower structural levels recorded maximum temperature conditions at lower pressures and higher temperatures than the metapelites in the upper structural levels. It is therefore suggested that the lower levels of the TGD experienced more important heating during D2, and that the thermal peak was attained at a later stage of their exhumation. In contrast, the overlap of calculated retrograde *P–T* conditions suggests that in both crustal levels the GASP reaction closed at equivalent depths after their tectonic juxtaposition during the exhumation of the Lower Unit.

## LOWER UNIT *P–T* PATH RECONSTRUCTION

Calculated *P–T* conditions agree with the metamorphic conditions and the *P–T* path deduced through phase equilibria in pelitic systems. The *P–T* diagrams in Fig. 12 also show the following relevant reaction boundaries discussed earlier: the 'dry' melting of muscovite (R1), the 'dry' melting of biotite (R2), orthopyroxene + melt appearance (R3) (Le Breton & Thompson, 1988; Spear 1993, figs 10–16), the upper pressure limit of the stability field of cordierite in peraluminous granitic melts (R5) (Vielzeuf & Holloway, 1988), and the univariant lines of the $Al_2SiO_5$ polymorph (calculated with TWEEQU).

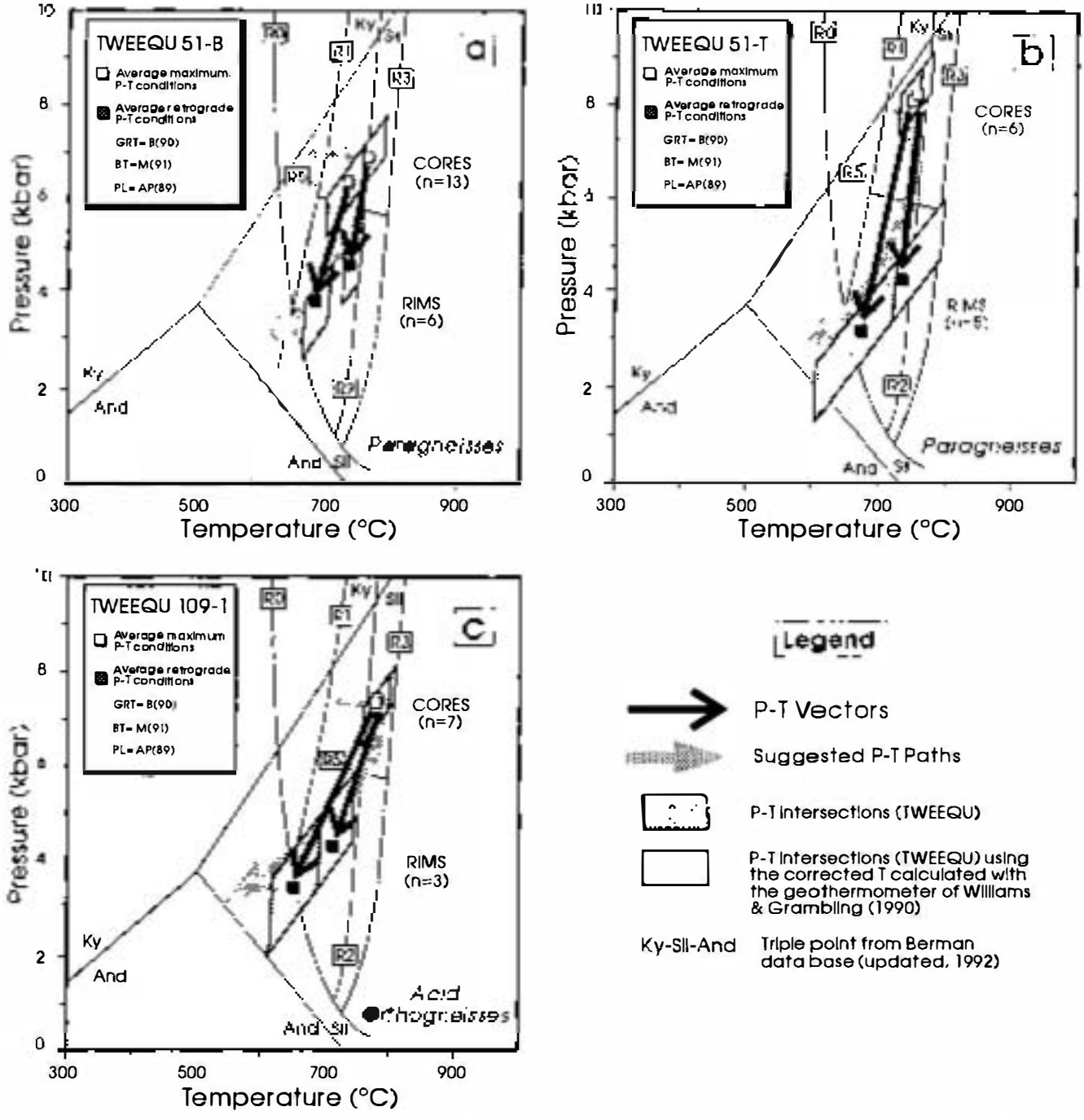


**Fig. 12.** TWEEQU results for maximum and retrograde $P$–$T$ conditions in (a) & (b) metapelites and (c) felsic orthogneisses. (R0): $H_2O$-saturated pelite solidus; (R1): Ms + Qtz + Pl = Sil + Kfs + L; (R2): Bt + Sill + Qtz + Pl = Grt + Kfs + L; (R3): Bt + Qtz + Pl = Opx + Kfs + L (after Le Breton & Thompson, 1988; Spear, 1993, figs 10–16); (R5): Bt + Sil + Qtz = Crd + Kfs + L (Vielzeuf & Holloway, 1988).

In all cases, the maximum $P$–$T$ conditions fall within the stability field of sillimanite, which is the aluminium silicate present in these rocks, and above the upper-$P$ limit of the stability of cordierite [(R5), Fig. 12). All calculated temperature conditions are higher than those required for the 'dry' melting of muscovite [(R1), Fig. 12]. For the metapelites of the upper structural levels, they are located slightly below, or at the biotite melting curve (R2), which is interpreted as being responsible for a large portion of melts in the study area. Calculated temperature conditions are lower than those required for reaction (R2) as located in Fig. 12. This may be due to a variety of factors, such as: (1) the approximate location of (R2) in $P$–$T$ space, which

can be shifted to lower temperatures in proportion to the albite content of plagioclase (Vielzeuf & Holloway, 1988) and by the addition of B, F and Cl to the melt (Le Breton & Thompson, 1988; Hensen & Osanai, 1994); (2) slight diffusional re-equilibration of garnet cores during early stages of cooling; and (3) since $T_{AP}$ values are lower than $T_{WG}$ values, it is possible that the WG thermometer is more appropriate for the composition of the garnet cores as well. The temperature conditions of the thermal peak recorded by the orthogneisses of the lower structural levels, whether the temperature correction is taken into consideration or not, are a few tens of degrees higher than those required for reaction (R2), but lower than (R3), therefore consistent with the absence of orthopyroxene in the study area. As can be seen in Fig. 12, the lengths and orientations of all the $P$–$T$ vectors imply a decompressional $P$–$T$ path that enters the stability field of cordierite, which has been commonly observed as a retrograde phase and within late peraluminous granites.

## TECTONOMETAMORPHIC IMPLICATIONS

In the Lower Unit of the TGD, gently dipping S2 mylonitic fabrics developed during different stages of M2 evolution, starting from the thermal peak. These fabrics were finally concentrated in the low-grade detachment zones located in the upper structural levels. A consistent shear sense has been documented from a majority of these non-coaxial fabrics by Escuder Viruete *et al.* (1994), with the upper structural levels being transported down to the south-east. The progressive variation in the style and geometry of D2 ductile deformation implies the tectonic exhumation of the Lower Unit, which represents mid-levels of orogenic crust, and is consistent with the structures expected to develop in a crustal-scale extensional shear zone, as suggested by Lister *et al.* (1984). The D2 event thus corresponds to a post-collisional crustal thinning stage which follows the D1 crustal thickening. A similar evolution has also been described in other parts of the Hercynian Belt of Central Europe (Dewey, 1988; Eisbacher *et al.*, 1989; Malavieille *et al.*, 1990; Faure *et al.*, 1990; Reinhardt & Kleeman, 1994; Brown & Dallmeyer, 1996).

The syn-D2 retrograde paths deduced for the Lower Unit from the sequence of mineral assemblages present in the metapelitic lithologies and from the thermobarometric data are consistent with each other. The resultant complete syn-D2 path for the Lower Unit (Fig. 13) has both of the basic characteristics of a path produced by tectonic denudation: an initial decompression phase followed by isobaric cooling, the latter caused by the thermal re-equilibration associated with the newly acquired structural position (Ruppel *et al.*, 1988). The existence immediately above the unit of the major boundary, which represents the tectonic contact with the Upper Unit, favours the interpretation that the thermal structure and a large part of the metamorphic evolution were controlled by the extensional movement of this tectonic contact. The syn-D2 tectonothermal evolution of the Lower Unit of the TGD is shown in the schematic sections of Fig. 14. The rocks studied initially equilibrated at the thermal peak at depths of the order of 25–30 km, under conditions of upper amphibolite facies, transitional to granulite facies; subsequently, rocks of the same structural levels developed S2 mylonitic fabrics in low-grade conditions. This indicates that the movement associated with the low-grade extensional-detachment shear-zone system caused the mobilization of at least 10 km of material situated structurally above the present upper boundary of the Lower Unit.

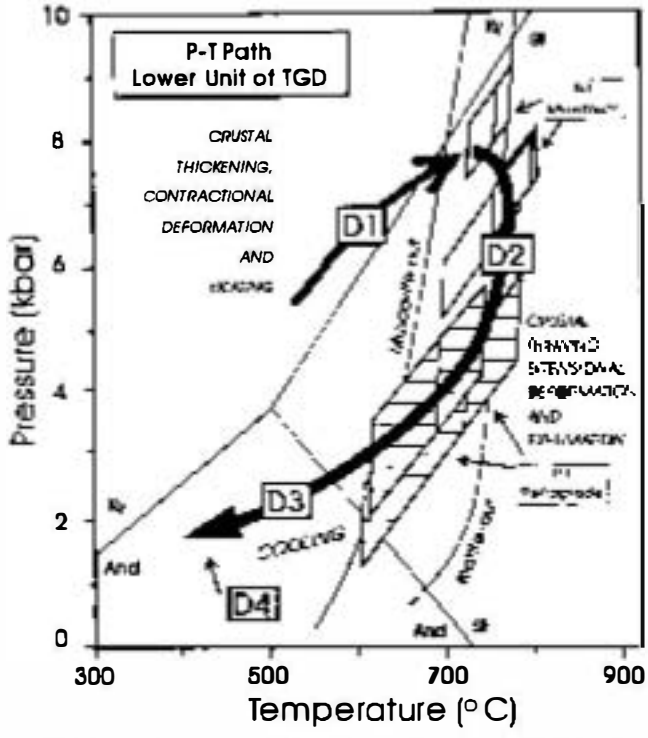


**Fig. 13.** $P$–$T$ path followed by the Lower Unit of the Tormes Gneissic Dome.

The $P$–$T$ vectors, the sequence deduced from melting reactions and the existence of two generations of mineralogically and structurally different anatectic leucogranites suggests that the migmatization in the Lower Unit occurred in two main pulses. Peraluminous leucogranites with garnet are interpreted to have formed close to the thermal peak, whereas peraluminous leucogranites with cordierite are interpreted to have formed during the decompression stage.

## CONCLUSIONS

The results of this study indicate that in the TGD a D1 contractional tectonothermal event, associated with crustal thickening during continental collision, was followed by a D2 event related to the extensional collapse of the previously thickened crust. The syn-D2

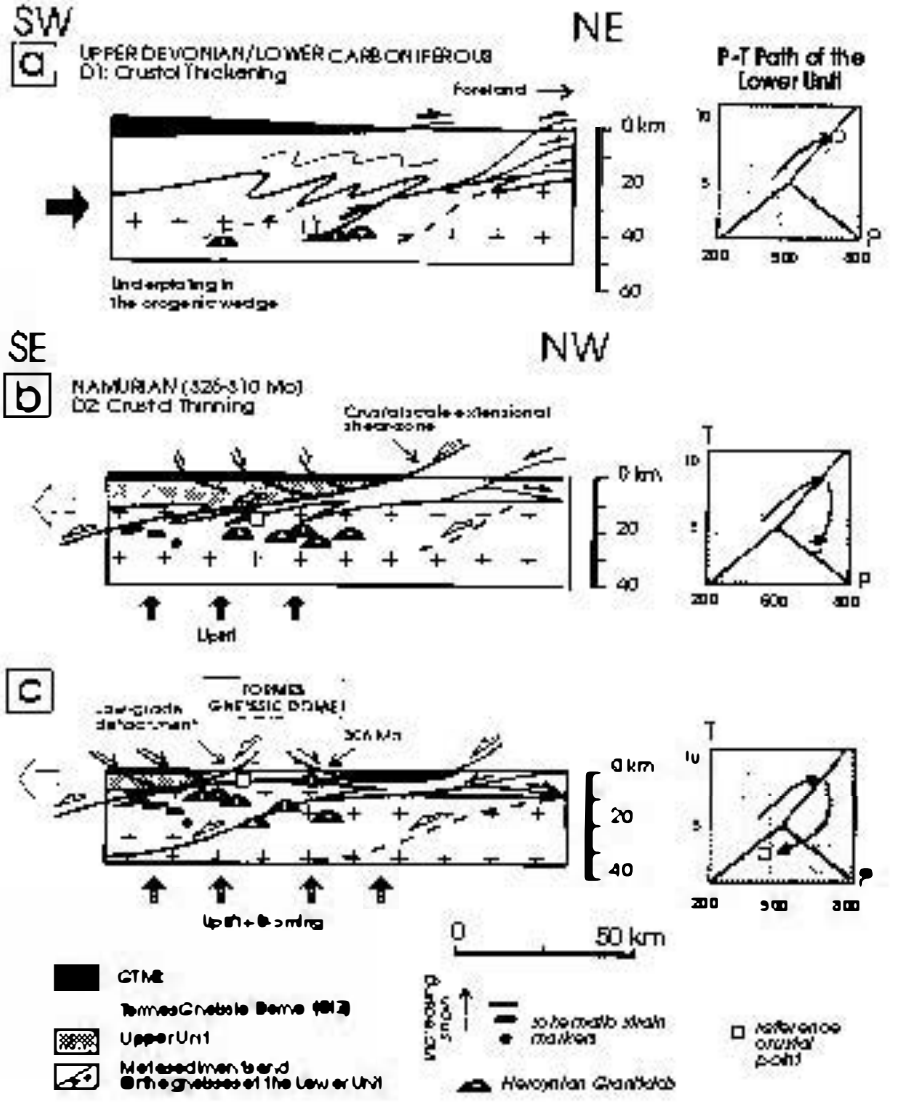


Fig. 14. A series of schematic sections showing the suggested tectonothermal evolution of the Tormes Gneissic Dome. The *P–T* path is that followed by a reference crustal level currently situated in the upper levels of the Lower Unit. Subsequent to the D1 contractional tectonics, which gave rise to thrust faults and nappe folds during the Upper Devonian/Lower Carboniferous and a M1 Barrovian metamorphism (a), a crustal-scale extensional shear zone initially accommodated the extensional collapse induced by the orogenic crustal thickening (b). The onset of the D2 extensional deformation in the Lower Unit coincided with the beginning of decompression under high-T conditions and, shortly afterwards, with the thermal peak of the M2 metamorphism and the generalized development of anatectic processes. During the subsequent drop in temperature, the deformation became concentrated in the low-grade detachment, which finally juxtaposed the Upper Unit over the Lower Unit. In advanced cooling stages (c), and as a consequence of the upward bowing of the extensional system, mainly induced by doming related to denudational tectonics, but probably also due to the emplacement of syntectonic plutons, the SE movement was transferred to a new branch of the low-grade detachment.

*P–T* path deduced for the Lower Unit is characterized by (1) an initial phase of decompression, related to tectonic exhumation and characterized by abundant anatexis, and (2) subsequent quasi-isobaric cooling associated with thermal re-equilibration in the new structural position. This *P–T* path is consistent with the tectonic transport along the dominant extensional shear zone and the later low-grade detachments, located in the upper structural levels of the unit, as well as with the tectonic juxtaposition of the Lower Unit against the Upper Unit. During the late D3 and D4 deformation events, the Lower Unit underwent cooling with mild decompression at a high crustal level, probably controlled by erosion processes.

## ACKNOWLEDGEMENTS

This paper represents part of the first author's PhD thesis research. We are very grateful to R. Rodriguez Fernández (ITGE) for his support during the field work, which was carried out in the framework of the MAGNA cartography program. The collaboration of

M. Lago from the Department of Earth Sciences of the University of Zaragoza, as well as the continuous scientific discussions with J. R. Martínez Catalán from the Department of Earth Sciences of the University of Salamanca, are also acknowledged. We thank J. Martignole and T. Rivers for an initial revision of the manuscript. We also thank M. Ballévre, M. Brown and F. Spear for comments and suggestions that helped to improve the quality of the final manuscript. Some aspects of this study received financial aid from projects DGICYT (MEC) PB91-0192-C02 and PB94-1396-C02, where part of the results of the research are contained. Permission to undertake laboratory work in Canada was given by G. Quinlan of the Memorial University of Newfoundland. M. Piranian, of the Electron Microprobe Laboratory of Memorial University, ensured an efficient microprobing environment during the course of this study.

## REFERENCES


Anovitz, L. M. & Essene, E. J., 1990. Thermobarometry and pressure–temperature paths in the Grenville Province of Ontario. *Journal of Petrology*, **31,** 197–241.

Aranovich, L. & Podlesskii, K. K., 1983. The cordierite-garnet-sillimanite-quartz equilibrium: experiments and applications. In: *Kinetics and Equilibrium in Mineral Reactions* (ed. Saxena, S.K.), pp. 173–189. Springer-Verlag, New York, NY.

Aranovich, L. & Podlesskii, K. K., 1989. Geothermobarometry of high-grade metapelites: simultaneously operating reactions. In: *Evolution of Metamorphic Belts* (eds Daly, J. S., Cliff, R. A. & Yardley, B.W.D). *Geological Society Special Publication*, **43,** 45–61.

Arenas, R., Gil Ibarguchi, J., González Lodeiro, F., Klein, E., Martínez Catalán, J., Ortega Girones, E., Pablo Maciá, J. de & Peinado, M., 1986. Tectonostratigraphic units in the complexes with mafic and related rocks of the NW of the Iberian Massif. *Hercynica*, **2,** 87–110.

Arenas, R., Rubio Pascual, F., Díaz García, F. & Martínez Catalán, J., 1995. High-pressure micro-inclusions and development of an inverted metamorphic gradient in the Santiago Schists (Ordenes Complex, NW Iberian Massif, Spain): evidence of subduction and syn-collisional decompression. *Journal of Metamorphic Geology*, **13,** 141–164.

Berman, R. G., 1990. Mixing properties of Ca-Mg-Fe-Mn garnets. *American Mineralogist*, **75,** 328–344.

Berman, R. G., 1991. Thermobarometry using multiequilibrium calculations: a new technique with petrologic applications. *Canadian Mineralogist*, **29,** 833–855.

Berman, R. G. & Koziol, A. M., 1991. Ternary excess properties of grossular-pyrope-almandine garnets and their influence in geothermobarometry. *American Mineralogist*, **76,** 1223–1231.

Brown, M. & Dallmeyer, R. D., 1996. Rapid Variscan exhumation and role of magma in core complex formation, southern Brittany metamorphic belt, France. *Journal of Metamorphic Geology*, **3,** 366–398.

Clemens, J. D. & Wall, V. J., 1981. Origin and crystallization of some peraluminous S-type granitic magmas. *Canadian Mineralogist*, **19,** 111–131.

Dewey, J. F., 1988. Extensional collapse of orogens. *Tectonics*, **7,** 1123–1139.

Diez Balda, M. A., Ayarza, P. & Martínez Catalán, J. R., 1992. El cizallamiento dúctil subhorizontal de la segunda fase hercínica al sur de Salamanca: engrosamiento y colapso extensional. *III Congreso Geologico de España, Simposios*, **2,** 365–374.

Diez Balda, M. A., Martínez Catalán, J. R. & Ayarza, P., 1995. Syn-collisional extensional collapse parallel to the orogenic trend in a domain of steep tectonics: the Salamanca Detachment Zone (Central Iberian Zone, Spain). *Journal of Structural Geology*, **17,** 163–182.

Doblas, M., López-Ruiz, J., Oyarzun, R., Mahecha, V., Sanchez Moya, Y., Hoyos, M., Cebriá, J. M., Capote, R., Hernández Enrile, J. L., Lillo, J., Lunar, R., Ramos, A. & Sopeña, A., 1994. Extensional tectonics in the central Iberian Peninsula during the Variscan to Alpine transition. *Tectonophysics*, **238,** 95–116.

Eisbacher, G., Luschen, E. & Wickert, F., 1989. Crustal scale thrusting and extension in the Hercynian Schwarzwald Vosges, Central Europe. *Tectonics*, **8,** 1–21.

Escuder Viruete, J., 1995. Evolución Tectonotermal del Domo Gneísico del Tormes, Salamanca, NO del Macizo Iberico. Implicaciones para la historia compresional y extensional de la Zona Centro Ibérica. *Unpubl. PhD Thesis, Universidad de Zaragoza. Spain.*

Escuder Viruete, J., Arenas, R. & Martínez Catalán, J. R., 1994. Tectonothermal evolution associated with Variscan crustal extension in the Tormes Gneissic Dome (NW Salamanca, Iberian Massif, Spain). *Tectonophysics*, **238,** 117–138.

Essene, E. J., 1989. The current status of thermobarometry in metamorphic rocks. In: *Evolution of Metamorphic Belts* (eds Daly, J.S, Cliff, J. A. & Yardley, B.W.D.). *Geological Society Special Publication*, **43,** 1–44.

Faure, M., Prost, A. E. & Lasne, E., 1990. Déformation ductile extensive d'âge namuro-westphalien dans le Plateau d'Aigurande, Massif Central Français. *Bulletin Societe Géologique France*, VI, **1,** 189–197.

Frost, B. R. & Chacko, T., 1989. The granulite uncentainty principe: limitations on thermobarometry in granulites. *Journal of Geology*, **97,** 435–450.

Fuhrman, M. L. & Lindsley, D. H., 1988. Ternary-feldspar modeling and thermometry. *American Mineralogist*, **73,** 201–216.

Gil Ibarguchi, J. I. & Martínez, F. J., 1982. Petrology of garnet-cordierite-sillimanite gneisses from the El Tormes Thermal Dome, Iberian Hercynian Fold belt (W Spain). *Contributions to Mineralogy and Petrology*, **80,** 14–24.

Hensen, J. & Osanai 1994. Experimental study of dehydration melting of F-bearing biotite in model pelitic compositions. *Mineralogical Magazine*, **58 A,** 410–411.

Julivert, M., Fontbote, J. M., Ribeiro, A. & Conde, L., 1972. *Mapa Tectónico de la Peninsula Ibérica y Baleares E., 1:1.000.000.* IGME, Madrid, Spain.

Kretz, R., 1983. Symbols for rock-forming minerals. *American Mineralogist*, **68,** 277–279.

Lancelot, J. R., Allegret, A. & Iglesias, M., 1985. Outline of Upper Precambrian and Lower Paleozoic evolution of the Iberian Peninsula according to U-Pb dating of zircons. *Earth and Planetary Science Letters*, **74,** 325–337.

Lasaga, C., 1983. Geospeedometry: An extension of geothermometry. In: *Kinetics and Equilibrium in Mineral Reactions* (ed. Saxena, S.K.), pp. 57–90. Springer-Verlag, New York, NY.

Le Breton, N. & Thompson, A. B., 1988. Fluid-absent (dehydration) melting of biotite in metapelites in the early stages of crustal anatexis. *Contributions to Mineralogy and Petrology*, **99,** 226–237.

Lister, G. S., Banga, G. & Feenstra, A., 1984. Metamorphic core complexes of Cordilleran type in the Cyclades, Aegean Sea, Greece. *Geology*, **12,** 221–225.

Lister, G. S. & Snoke, A. W., 1984. S-C Mylonites. *Journal of Structural Geology*, **6,** 617–638.

Lonker, S. W., 1981. The P-T-X relations of the cordierite-garnet-sillimanite-quartz equilibrium. *American Journal of Science*, **281,** 1056–1090.

López Plaza, M. & Gonzalo, J. C., 1993. Caracterización geoquímica de las anatexitas del Domo del Tormes (provincias de Salamanca y Zamora). *Revista Sociedad Geológica de España*, **6,** 3–4.

Malavieille, J., Guihot, P., Cta, S., Lardeaux, J. M. & Gardien, V., 1990. Collapse of the thickened Variscan crust in the French Massif Central: Mont Pilat extensional shear zone

and St. Etienne Late Carboniferous basin. In: *Terranes in the Variscan Belt of Europe and Circum-Atlantic Paleozoic Orogens* (ed. Matte, Ph.). *Tectonophysics*, **177**, 139–149.

Martínez, F. J., 1974. Estudio del área metamórfica del NW de Salamanca (Cordillera Herciniana, España). *Trabajos de Geología*, **7**, 3–59.

Martínez, F. J., Jolivert, M., Sebastian, A., Arboleya, M. L. & Gil-Ibarguchi, J. I., 1988. Structural and thermal evolution of high-grade areas in the northwestern parts of the Iberian Massif. *American Journal of Science*, **28**, 969–996.

McMullin, D., Berman, R. G. & Greenwood, H. J., 1991. Calibration of the SGAM thermobarometer for pelitic rocks using data from phase equilibrium experiments and natural assemblages. *Canadian Mineralogist*, **29**, 889–908.

Nisbet, E. G. & Fowler, C.R (eds), 1988. Heat, Metamorphism, and Tectonics. *Mineralogical Association of Canada, Short Course Notes*, **14**.

Peacock, S. M., 1989. Thermal modeling of metamorphic Pressure-Temperature-Time Paths: a forward approach. In: *Metamorphic Pressure-Temperature-Time Paths* (eds Spear, F. S. & Peacock, S. M.), pp. 57–102. *Short Course in Geology*, American Geophysical Union, Washington, DC, USA.

Pérez Estaún, A., Martínez Catalán, J. R. & Bastida, F., 1991. Crustal thickening and deformation sequence in the footwall to the suture of the Variscan belt of Northwest Spain. *Tectonophysics*, **191**, 243–253.

Perkins, E. H., Brown, T. H. & Berman, R. G., 1987. PTX-SYSTEM: Three programs for calculation of pressure-temperature-composition phase diagrams. *Computer & Geosciences*, **12**, 749–755.

Platt, J. P. & Vissers, R. L. M., 1980. Extensional structures in anisotropic rocks. *Journal of Structural Geology*, **2**, 397–410.

Reinhardt, J. & Kleeman, U., 1994. Extensional unroofing of granulitic lower crust and related low-pressure, high temperature metamorphism in the Saxonian Granulite Massif, Germany. *Tectonophysics*, **238**, 71–94.

Rumble, D., 1973. Fe-Ti oxide minerals from regionally metamorphosed quartzites of Western New Hampshire. *Contributions to Mineralogy and Petrology*, **42**, 181–195.

Ruppel, C, Royden, L. & Hodges, V., 1988. Thermal modeling of extensional tectonics: Application to pressure-temperature-time histories of metamorphic rocks. *Tectonics*, **7**, 947–957.

Selverstone, J. & Chamberlain, C. P., 1990. Apparent isobaric cooling paths from granulites: two counterexamples from British Columbia and New Hampshire. *Geology*, **18**, 307–310.

Serrano Pinto, M. & Gil Ibarguchi, J. I., 1987. Revisión de los datos geocronológicos e isotópicos de granitoides hercínicos y ante-hercínicos de la Región Galaico-Castellana. *Memoria Museu Laboratorio Mineralogía y Geología*, **1**, 171–186.

Spear, F. S., 1989. Petrologic determination of metamorphic Pressure-Temperature-Time paths. In: *Metamorphic Pressure-Temperature-Time Paths* (eds Spear, F. S. & Peacock, S.M.) pp. 1–56. *Short Course in Geology*, American Geophysical Union.

Spear, F. S., 1991. On the interpretation of peak metamorphic temperatures in light of garnet diffusion during cooling. *Journal of Metamorphic Geology*, **9**, 379–388.

Spear, F. S., 1993. *Metamorphic Phase Equilibria and Pressure-Temperature-Time Paths*. Mineral Society of America, Monograph, Washington, DC.

Spear, F.S & Florence, F. P., 1992. Thermobarometry in granulites: pitfalls and new approaches. *Precambrian Research*, **55**, 209–241.

Spear, F. S., Hickmott, D. D. & Selverstone, J., 1990. Metamorphic consequences of thrust emplacement, Fall Mountain, New Hampshire. *Geological Society of America Bulletin*, **102**, 1344–1360.

Spear, F. S., Kohn, M. J., Florence, P. & Menard, T., 1991. A model for garnet and plagioclase growth in pelitic schists: implications for thermobarometry and P-T path determinations. *Journal of Metamorphic Geology*, **8**, 683–696.

Spear, F. S. & Selverstone, J., 1983. Quantitative P-T paths from zoned minerals: Theory and tectonic applications. *Contributions to Mineralogy and Petrology*, **83**, 348–357.

Thompson, A. B. & England, P. C., 1984. Pressure-temperature-time paths of regional metamorphism of thickened continental crust. II. Some petrological constraints from mineral assemblages in metamorphic rocks. *Journal of Petrology*, **25**, 929–955.

Vielzeuf, D. & Holloway, J. R., 1988. Experimental determination of fluid-absent melting relations in the pelitic system. Consequences for crustal differentiation. *Contributions to Mineralogy and Petrology*, **98**, 257–276.

Williams, M. L. & Grambling, J. A., 1990. Manganese, ferric iron, and the equilibrium between garnet and biotite. *American Mineralogist*, **75**, 886–908.

*Received 30 July 1996; revision accepted 30 March 1997.*